

 Open access • Posted Content • DOI:10.1101/2020.11.17.387134

Universal annotation of the human genome through integration of over a thousand epigenomic datasets — [Source link](#)

Vu H, Jason Ernst

Institutions: University of California, Berkeley

Published on: 19 Nov 2020 - bioRxiv (Cold Spring Harbor Laboratory)

Topics: Genome project and Annotation

Related papers:

- [StateHub-StatePaintR: rules-based chromatin state annotations.](#)
- [StateHub-StatePaintR: rapid and reproducible chromatin state evaluation for custom genome annotation](#)
- [A Statistical Framework to Predict Functional Non-Coding Regions in the Human Genome Through Integrated Analysis of Annotation Data](#)
- [iLoci: Robust evaluation of genome content and organization for provisional and mature genome assemblies](#)
- [Ultrafast and scalable variant annotation and prioritization with big functional genomics data.](#)

Share this paper:    

View more about this paper here: <https://typeset.io/papers/universal-annotation-of-the-human-genome-through-integration-1ptf9v6pyv>

Universal annotation of the human genome through integration of over a thousand epigenomic datasets

Ha Vu^{1,2}, Jason Ernst^{1,2,3,4,5,6,7}

¹ Bioinformatics Interdepartmental Program, University of California, Los Angeles, CA, 90095, USA.

² Department of Biological Chemistry, University of California, Los Angeles, Los Angeles, CA 90095, USA

³ Eli and Edythe Broad Center of Regenerative Medicine and Stem Cell Research at University of California, Los Angeles, Los Angeles, CA 90095, USA

⁴ Computer Science Department, University of California, Los Angeles, Los Angeles, CA 90095, USA

⁵ Jonsson Comprehensive Cancer Center, University of California, Los Angeles, Los Angeles, CA 90095, USA

⁶ Molecular Biology Institute, University of California, Los Angeles, Los Angeles, CA 90095, USA

⁷ Department of Computational Medicine, University of California, Los Angeles, Los Angeles, CA 90095, USA

Abstract

Genome-wide maps of chromatin marks such as histone modifications and open chromatin sites provide valuable information for annotating the non-coding genome, including identifying regulatory elements. Computational approaches such as ChromHMM have been applied to discover and annotate chromatin states defined by combinatorial and spatial patterns of chromatin marks within the same cell type. An alternative ‘stacked modeling’ approach was previously suggested, where chromatin states are defined jointly from datasets of multiple cell types to produce a single universal genome annotation based on all datasets. Despite its potential benefits for applications that are not specific to one cell type, such an approach was previously applied only for small-scale specialized purposes. Large-scale applications of stacked modeling have previously posed scalability challenges. In this paper, using a version of ChromHMM enhanced for large-scale applications, we applied the stacked modeling approach to produce a universal chromatin state annotation of the human genome using over 1000 datasets from more than 100 cell types, denoted the full-stack model. The full-stack model states show distinct enrichments for external genomic annotations, which we used in characterizing each state. Compared to cell-type-specific annotations, the full-stack annotation directly differentiates constitutive from cell-type-specific activity and is more predictive of locations of external genomic annotations. Overall, the full-stack ChromHMM model provides a universal chromatin state annotation of the genome and a unified global view of over 1000 datasets. We expect this to be a useful resource that complements existing cell-type-specific annotations for studying the non-coding human genome.

Introduction

Genome-wide maps of histone modifications, histone variants and open chromatin provide valuable information for annotating the non-coding genome features, including various types of regulatory elements [1–5]. These maps -- produced by assays such as chromatin immunoprecipitation followed by high-throughput sequencing to map histone modifications or DNase-seq to map open chromatin-- can facilitate our understanding of regulatory elements and genetic variants that are associated with disease [6–12]. Efforts by large scale consortia as well as many individual labs have resulted in these maps for many different human cell and tissue types for multiple different chromatin marks [1,9,13–20].

The availability of maps for multiple different chromatin marks in the same cell or tissue type motivated the development of methods such as ChromHMM and Segway that learn ‘chromatin states’ based on the combinatorial and spatial patterns of marks in such data [21–23]. These methods then annotate genomes in a cell-type-specific manner based on the learned chromatin states. They have been applied to annotate more than a hundred diverse cell and tissue types [3,16,24]. Previously, large collections of cell-type-specific annotations have been generated using either (1) independent models that learn a different set of states in each cell or tissue type or (2) a model that is learned across all cells and tissues, resulting in a common set of states across cell types, yet generating cell-type-specific state annotations. This latter approach has previously been referred to as a ‘concatenated’ approach (**Supp. Fig. 1**) [22,25]. Variants of this approach allow information from other cell types to influence the state annotations in one cell type at a position, but still produce cell-type-specific state annotations [26,27]. These models that produce cell-type-specific annotations are natural for cell-type-specific analyses.

A complementary approach to applying ChromHMM to data across multiple different cell types referred to as the ‘stacked’ modeling approach was also previously suggested (**Supp. Fig. 1**) [22,25]. Instead of learning cell-type-specific annotations based on a limited number of datasets per cell type, the stacked modeling approach learns a single universal genome annotation based on the combinatorial and

spatial patterns in datasets from multiple marks across multiple cell types. This approach differs from the concatenated and independent modeling approaches as those approaches only identify combinatorial and spatial patterns present among datasets within one cell type.

Such a universal annotation from stacked modeling provides potential complementary benefits to existing cell-type-specific chromatin state annotations. First, stacked models may help differentiate regions with constitutive chromatin activities from those with cell-type-specific activities. Previously, specific chromatin states from ‘concatenated’ cell-type-specific annotations were post-hoc clustered to analyze chromatin dynamics across cell and tissue types, yet such an approach does not provide a systematic and global view of the dynamics of all the data [3,16]. Second, the stacked modeling approach bypasses the need to pick a specific cell or tissue type when analyzing a single partitioning and annotation of the genome. Focusing on a single cell or tissue type may not be desirable for many analyses involving other annotations that are not inherently cell-type-specific, such as those involving conserved DNA sequence or genetic variants. Alternatively, compared to analyzing chromatin state annotations across all cells or tissue types, while the stacked model state definitions are more complex, the resulting genome annotations are simpler and non-overlapping. With the stacked modeling, each location is simply assigned to one of N universal states, whereas in the concatenated model, each location is assigned to one of M states in K cell types. The value of N can be selected to be much smaller than the number of possible combinations of chromatin state annotations across cell types at a location with the concatenated modeling, M^K , as well as the number of possible combinations of cell types and states, M^K . Finally, annotations by the stacked modeling leverages a larger set of data for annotation, and thus has the potential to be able to identify genomic elements with greater sensitivity and specificity.

Despite the potential complementary advantages of the ‘stacked’ modeling approach, it has only been applied on a limited scale to combine data from a small number of cell types for highly specific purposes [28,29]. No large-scale application of the stacked modeling approach to many diverse cell and tissue types has been previously demonstrated. This may have in part been due to large-scale applications of stacked modeling raising scalability challenges not present in cell-type-specific modeling.

Here, we present a large-scale application of the stacked modeling approach with more than a thousand human epigenomic datasets as input, using a version of ChromHMM of which we enhanced the scalability. We conduct various enrichment analyses on the states resulting from the stacked modeling and give biological interpretations to them. We show that compared to the cell-type-specific annotations, the stacked model's annotation shows greater correspondence to various external genomic annotations not used in the model learning. We analyze the states in terms of enrichment with different types of genetic variants, and highlight specific states of the stacked model that are enriched with phenotypically associated genetic variants. Additionally, we identify specific states enriched with cancer-associated somatic mutations. We expect the stacked model annotations and detailed characterization of the states that we provide will be a valuable resource for studying the epigenome and non-coding genome, complementing existing cell-type-specific annotations.

Results

Annotating the human genome into universal chromatin states

We used the stacked modeling approach of ChromHMM to produce a universal chromatin state annotation of the genome based on data from over 100 cell and tissue types from the Roadmap Epigenomics and ENCODE projects (**Fig. 1**) [14,16]. In total we applied ChromHMM to 1032 datasets for 30 histone modifications, a histone variant (H2A.Z), and DNase I hypersensitivity (**Supp. Fig. 2**). The set of cell and tissue types were the same as those for which cell-type-specific annotations were previously generated by applying the ‘concatenated’ modeling approach of ChromHMM [22,25]. We note that not all chromatin marks were profiled in all cell or tissue types, but the stacked modelling can still be applied directly.

We focused our analysis on a model with 100 states. We used a larger number of states than typically used for cell-type-specific models to reflect the greater information available when defining states based on data from many cell types. At the same time, we limited the model to 100 states to ensure manageable biological interpretation of different states (**Supp. Fig. 3**) (**Methods**). We denote the model’s output chromatin state annotation the ‘full-stack’ genome annotation.

Major groups of full-stack states

We characterized each state of the model by analyzing the model parameters (emission probabilities and transition probabilities) and state enrichments for other genome annotations (**Fig. 2, 3A, Supp. Fig. 4-7**). The other genomic annotations include previous cell-type-specific chromatin state annotations (**Supp. Fig. 8**), cell-type-specific gene expression data (**Supp. Fig. 9-10**), and various independent existing genomic annotations (**Fig. 3A**). These independent genomic annotations included annotated gene features, evolutionary constrained elements, and assembly gaps, among others (**Methods**).

These analyses led us to group the 100 full-stack states into 16 groups (**Fig. 2A**). One group includes states associated with assembly gaps (state GapArtf1) and alignment artifacts (states GapArtf2-3). Some other groups are associated with repressive or inactive states, including quiescent states (states Quies1-5) (low emissions of all experiments, except possibly weak signals in H3K9me3), heterochromatin

states associated with H3K9me3 (states HET1-9), and polycomb repressed states associated with H3K27me3 (states ReprPC1-9). There is an acetylations group marked primarily by high emission of various acetylation marks (states Acet1-8). We also formed active and weak candidate enhancers groups (states EnhW1-8 and EnhA1-20, respectively) associated with H3K4me1, DNase, H2A.Z, and/or H3K27ac. Four groups are associated with transcriptional activities, including a group of transcribed enhancers (states TxEnh1-8), two groups of weak or strong transcription (states TxWk1-2, Tx1-8, respectively), and one group associated with exon and transcription (states TxEx1-4). These transcriptional activities groups are associated with at least one of these marks H3K36me3, H3K79me1, H3K79me2, and H4K20me1. Another group consists of two zinc finger (ZNF) gene states associated with H3K36me3 and H3K9me3 (states ZNF1-2). A DNase group consists of one state (DNase1) with strong emission of only DNase in all profiled cell types. Three groups are associated with promoter activities, marked by emission of some promoter marks such as H3K4me3, H3K4me2, and H3K9ac. One promoter group was of bivalent states associated with promoter marks and H3K27me3 (states BivProm1-4). The other two promoter groups were flanking promoter states (PromF1-7) and transcription start sites (TSS) states (TSS1-2) where the flanking promoter states also show emission of H3K4me1.

Enrichments for external annotations supported these state groupings (**Fig. 3A**), as well as further distinctions or characterizations among states within each group. For example, the state in the assembly gap group (GapArt1) had ~8 fold enrichment for assembly gaps and contained 99.99% of all assembly gaps (**Fig. 3A**). The states in the zinc finger gene group, ZNF1-2, had 20.8 and 68.6 fold enrichment for zinc finger named genes, respectively (**Fig. 3A**). States in the transcription groups (TxEnh1-8, TxWk1-2, Tx1-8, TxEx1-4) were all at least 2.1 fold enriched for annotated genes, which covered 88.8–97.5% of the states. These states are associated with higher expression of genes across different cell types, particularly when downstream of their TSS (**Fig 3A, C, Supp. Fig. 9-10**). Distinctions were seen among these states, for example, in terms of their positional enrichments relative to TES (**Fig. 3A, D, Supp. Fig. 11**). States in the flanking promoter group (PromF1-7) showed 6.5-28 fold enrichment for being within 2kb of annotated TSS, and genes whose TSS regions overlapped these states had higher average gene expression across

different cell types (**Fig. 3A, C, Supp. Fig. 9-10**). These states differed among each other in their enrichments with upstream or downstream regions of the TSS (**Fig. 3E, Supp. Fig. 11**). The states in the transcription start site group (TSS1-2) had particularly high enrichments around the TSS, with ≥ 100 fold enrichment (**Fig. 3A, E**). The DNase specific group, which comprised of the state DNase1, showed strong enrichment for CTCF-specific chromatin states defined in six cell types [30] (**Fig. 3F, Supp. Fig. 12**). A detailed characterization of all states can be found in **Supplementary Data**.

Stacked Model Differentiates Cell-Type-Specific from Constitutive Activity

While the major groups of states outlined above can correspond to states in cell-type-specific models [3,16], the full-stack states provide additional information. For example, the states directly differentiate cell-type-specific from constitutive activities. Consistent with previous findings that enhancers tend to be relatively cell-type-specific while promoters tend to be shared across cell types [3,31], enhancer states exhibited clearer cell-type-specific associations than those of the promoter states (**Figure 2C, Supplementary Data**). This is also reflected in the states' coefficients of variation across different cell groups in terms of emission probabilities for the marks DNase, H3K27ac, H3K4me1, H3K4me2, H3K4me3 and H3K9ac. On average, states of enhancer and weak enhancer groups (EnhW1-8, EnhA1-20) show at least two fold higher of the coefficients of variations compared to states in the TSS, flanking promoter and bivalent promoters groups (TSS1-2, PromF1-7, BivProm4) (**Supp. Fig. 13**). The enhancer states differed among each other in their associations with different cell/tissue types such as brain (EnhA6), blood (EnhA7-9 and EnhWk6), digestive tissue (EnhA14-15), and embryonic stem cells (EnhA18) (**Fig. 1-2, Supp. Fig. 14-15**). These differences in cell-type-specific activities are also associated with different gene expression levels of overlapping genes with the states. For example, some blood enhancer states (EnhA8, EnhA9, EnhWk6) overlapped genes with higher average gene expression in cell types of the blood group, while some enhancer states specific to digestive group or liver tissues (EnhA14, EnhA15) showed higher gene expression in the corresponding cell or tissue types (**Fig. 3C, Supp. Fig. 9**).

Other groups of states besides enhancers also had individual states with cell-type-specific differences. For example, four of the nine states in the heterochromatin group show higher emission probabilities of H3K9me3 in only subsets of cell types (states HET1-2 with IMR90 and Epithelial cells; state HET4 with adipose, mesench, neurospheres, ESC, HSC&B-cells; state HET9 with ESC/iPSC) (**Supplementary Data**). In addition, some quiescent states (Quies1-2, Quies4-5) show weak signals of H3K9me3 in specific groups of cell types (**Supplementary Data**). States in the polycomb repressed and bivalent promoter groups (ReprPC1-9, BivProm1-4) also show differences in signals across cell groups, such as state ReprPC9, which showed H3K27me3 signals in only ESC/iPSC cell types (**Supplementary Data**). The ability of the stacked modeling approach to explicitly annotate both cell-type-specific and constitutive patterns for diverse classes of chromatin states highlights an advantage of this approach relative to the concatenated modeling.

Full-stack states are more predictive of external annotations than cell-type-specific models

Another benefit of the stacked modeling approach is its ability to more accurately identify genomic elements shared across cell and tissue types. To demonstrate this, we compared the full-stack state annotation against two sets of cell-type-specific chromatin state annotations in terms of recovering locations of various external genome annotations (**Methods**). One set was the previously published 18-chromatin state annotations defined in 98 cell or tissue types (equivalently, reference epigenomes) using a common set of six chromatin marks from Roadmap Epigenomics with the concatenated modeling approach [16]. The other set of annotations we compared the full-stack annotation against were 100-state cell-type-specific annotations that we generated separately for each of the 127 cell or tissue types using all available chromatin marks in the respective cell or tissue type (**Methods**).

The external genome annotations we used for the evaluations included locations of coding sequences, assembly gaps, CpG Islands, lamina associated domains (laminB1lads), PhastCons elements, pseudogenes, exons, gene body, transcription end sites, transcription start sites and the 2kb neighboring regions, repeat elements, and zinc finger named (ZNF) genes. The full-stack annotation resulted in the best

AUROC (area under the receiver operating curve) in predicting all genomic annotations compared to the previous 18-state cell-type-specific annotations across all cell types (**Supp. Fig. 16-17**). The full-stack model also showed the best AUROC in recovering locations of these genomic annotations for 10 of 13 evaluations compared to all 100-state cell-type-specific annotations (**Fig. 4**). The only evaluations in which the full-stack model did not outperform all 100-state cell-type-specific models were those involving assembly gaps, laminB1lads, and ZNF genes (**Fig. 4B, Supp. Fig. 18**), where at most 6 of the 127 100-state cell-type-specific models performed better. Additionally, we obtained similar results in comparing full-stack annotations with cell-type-specific annotations in predicting CTCF specific chromatin states in multiple cell types, where the full-stack annotation resulted in highest AUROC in all cases (**Supp. Fig. 19**).

Overall, these results demonstrate the benefits of full-stack chromatin state annotations, which showed better predictive power in recovering the locations of a variety of independent genomic annotations. The increased predictive power of the stacked modeling approach can be attributed to it taking into account information from more datasets that cover a large number of cell types when inferring state annotations.

Full-stack states show distinct enrichments for repeat elements

As the full-stack model showed greater predictive power for repeat elements than cell-type-specific models (**Fig. 4A, Supp. Fig. 29-31**), we next analyzed which states contributed most to this power. The full-stack state enrichments for bases in repeat elements ranged from 10-fold depletion to 2-fold enrichment (**Fig. 3A**). The top ten states most enriched with repeat elements were chromatin states that were associated with H3K9me3 marks and in the heterochromatin, artifact, quiescent, or ZNF genes groups (**Fig. 5A-B**).

We also observed that individual full-stack states had distinct enrichments for different repeat classes (**Fig. 5C, Supp. Fig. 20**). For example, Acet1, a state associated with various acetylation marks and H3K9me3 had a 23-fold enrichment for simple repeats (**Supp. Fig. 20**). The two states in the artifact group, GapArtf2-3, had a particularly high enrichment for satellite (181 and 145 fold, respectively) and rRNA repeat classes (75 and 580 fold, respectively) (**Fig. 5C, Supp. Fig. 20**). States in the transcription start site group, TSS1-

2, were most strongly enriched with tRNA and low complexity repeat class (~10-60 fold) (**Supp. Fig. 20**). We also saw specific states associated with the largest repeat classes of the genome, SINEs, LINEs, and LTRs. SINE repeats were most enriched in state Tx5 (3.7 fold) (**Fig. 5C**), which had high emission of H3K36me3 (**Fig. 2A-B, Supp. Fig. 4-5**). LINEs and LTRs repeats were most enriched for states in the H3K9me3-associated heterochromatin group with LINE most enriched in HET3 (3.4 fold), while LTRs were most enriched in HET5 (4.7 fold) (**Fig. 5C, Supp. Fig. 20**). We also confirmed that the increased predictive power of the full-stack model over cell-type-specific models, which was previously seen for repeat elements overall, also held for most of the individual repeat classes (**Supp. Fig. 21**).

Full-stack states show distinct enrichments for constrained elements and conservation states

Sequence constrained elements are another class of genomic elements that are not cell-type-specific and for which the full-stack model showed greater predictive power than the cell-type-specific models (**Fig. 4B, Supp. Fig. 16-18**). We next sought to better understand the relationship between full-stack states and sequence conservation annotations. We observed 10 states that had at least a 3.4 fold enrichment for PhastCons elements (**Fig. 5A**). These states were associated with the TSSs or being proximal to them (TSS1-2 and PromF4-5), transcription with strong H3K36me3 signals (TxEx2 and TxEnh4), or enhancers associated with mesenchymal, muscle, heart, neurosph, adipose (EnhA2) (**Fig. 5A-B**). In contrast, seven states (HET3-4,6-7,9, Quies4, Gap Artf2) were more than two fold depleted for PhastCons elements, which all had more than a 1.5 fold enrichment for repeat elements (**Fig. 5A**).

To gain a more refined understanding of the relationship between the full-stack chromatin states and conservation, we analyzed their enrichment using 100 previously defined conservation states by the ConSHMM method [32]. These conservation states were defined based on the patterns of other species' genomes aligning to or matching the human reference genome within a 100-way vertebrate alignment. We observed 29 different conservation states maximally enriched for at least one full-stack state (**Fig. 3B, Supp. Fig. 22-23**).

These states included, for example, ConsHMM state 1, a conservation state corresponding to bases aligning and matching through all vertebrates and hence most associated with constraint. ConsHMM state 1 had ≥ 10 fold enrichment for exon associated full stack states TxEx1-4 and TxEnh4 (**Supp. Fig. 22**). Another ConsHMM state, state 28, which is associated with moderate aligning and matching through many vertebrates and strongly enriched around TSS and CpG islands, had a 44.5 and 47.8 fold enrichment for TSS-associated full-stack states TSS1 and TSS2, respectively (**Supp. Fig. 22**). Additionally, this conservation state is consistently the most enriched conservation state for full stack states associated with flanking and bivalent promoters (**Fig. 3B, Supp. Fig. 22**). ConsHMM state 2, which has high aligning and matching frequencies for most mammals and a subset of non-mammalian vertebrates and previously associated with conserved enhancer regions [32], showed >2.7 fold enrichment for some full-stack enhancer states for Brain (EnhWk4 and EnhA6), ESC & iPSC (EnhA17,19 and EnhWk8), neurosph (EnhWk4, EnhA2,17), and mesenchymal, muscle, heart, adipose (EnhA2) (**Fig. 3B, Supp. Fig. 22**).

ConsHMM state 100, a conservation state associated with alignment artifacts, was 10.9 folds enriched for full-stack state ZNF1, which showed 20.8 fold enrichment with ZNF genes (**Fig. 3A-B, Supp. Fig. 22**). This is consistent with previous analysis using cell-type-specific annotations showing that ConsHMM state 100 was enriched in a ZNF gene-associated chromatin state [32]. Interestingly though, another full-stack state (ZNF2) that was even more strongly enriched for ZNF genes (68.6 folds), had 0.4 fold enrichment for ConsHMM state 100, and instead was most enriched with ConsHMM state 1 (**Fig. 3A-B, Supp. Fig. 22**). Therefore, the full-stack annotation helped distinguish two ZNF-gene associated states that are associated with distinct conservation states. As this example illustrates, the full-stack annotation captured conservation state enrichments that were generally consistent with those seen in cell-type-specific annotations, but could also identify additional refined enrichment patterns.

Specific full stack states show distinct enrichments and depletions for structural variants

We also analyzed the enrichment of the full-stack states for overlap with structural variants (SVs) mapped in 17,795 deeply sequenced human genomes [33]. We focused on the two largest classes of SVs, deletions

and duplications, that were previously analyzed using 15-state cell-type-specific chromatin state models [16,33]. In those analyses, enrichments were computed for 1-kb windows that were stratified based on the number of cell or tissue types each state was present. ZNF gene and heterochromatin states were enriched for deletions and duplications, with the enrichments being strongest when bases were annotated as those states in larger numbers of cell or tissue types [33].

Consistent with those previous results, using the full-stack model, we observed that of the 13 states that were in the top 10 maximally enriched states with either deletions or duplications (1.18 fold or greater), seven were in the heterochromatin group (HET1-2,4-7,9) and one was in the ZNF gene state (ZNF2) (**Fig. 6A, Supp. Fig. 24**). The other five states included one artifact state (GapArtf2), three quiescent states (Quies1-2,4) and a polycomb repressed state (ReprPC8) (**Fig. 6A**). The quiescent states Quies1-2,4, despite the generally low frequencies for all marks, did have higher emission probabilities for H3K9me3 compared to other chromatin marks (**Fig. 6B**). While the full-stack states showed generally consistent patterns of enrichments with the analysis of [33], it allowed a more refined analysis of enrichment patterns with structural variants. For example, it identified a polycomb repressed state (ReprPC8) that was enriched with duplication (1.21 fold enriched) and yet depleted with deletions (5 fold depleted) (**Fig. 6A**).

The full-stack model was also more predictive of SV than cell-type-specific annotations. In comparing with cell-type-specific annotations, the full-stack model had better AUROCs for predicting locations of deletions and duplications than the 18-state model in all cases, and the 100-state cell-type-specific model in all cases except for two out of 127 cell-types (**Supp. Fig. 25-26**). Additionally, we verified that the full-stack model had higher AUROC in predicting duplications and deletions compared to annotations obtained by ranking genomic bases based on the number of cell or tissue types that a state was observed separately for each state in the 15-state model, as in the approach of [33] (**Methods, Supp. Fig. 27**). These results show that the full-stack annotation can uncover enrichment patterns with SVs that are consistent with cell-type-specific annotations, yet highlight states with greater predictive power and offer a more refined chromatin annotation of the regions enriched with SVs.

Full stack-state gives insights into bases prioritized by different variant prioritization scores

Various scores have been proposed to prioritize deleterious variants in non-coding regions of the genome or genome-wide. These scores are based on either conservation or on integrating diverse sets of genomic annotations. Though the scores all serve to prioritize variants, they can vary substantially from each other and it is often not clear the differences among the types of bases that different scores prioritize. To better understand the epigenomic contexts of bases that each score tends to prioritize, we analyzed the full-stack state enrichment for bases they prioritize. As the scores we considered are not specific to a single cell type, the full-stack states have the potential to be more informative for this analysis than cell-type-specific annotations. We considered a set of 14 different variant prioritization scores that were previously analyzed in the context of conservation state analysis [32]. The 14 scores for which we analyzed prioritized variants in non-coding regions were CADD(v1.4), CDTS, DANN, Eigen, Eigen-PC, FATHMM-XF, FIRE, fitCons, FunSeq2, GERP++, LINSIGHT, PhastCons, PhyloP, and REMM [34–46]. For each of these scores, we first analyzed the full-stack state enrichments for the top 1% prioritized non-coding variants relative to the background of non-coding regions on the genome (**Methods**).

In the top 1% prioritized non-coding bases, 19 states were among the top five most enriched states ranked by at least one of the 14 scores (**Fig. 6C, Supp. Fig. 28, 29**). These 19 states include six states in flanking promoter and TSS groups, three states in the bivalent promoter group, five states in enhancers and transcribed enhancers groups, three states in the exon-associated transcription group, one polycomb repressed state, and one DNase state (**Fig. 6C**). Seven scores (DANN, Eigen, Eigen_PC, funSeq2, CDTS, CADD and REMM) had their top five enriched states exclusively associated with promoter and TSS states (PromF2-5, TSS1-2, BivProm1-2,4), with enrichments ranging between 8.6 and 70 fold (**Fig. 6C**). Some other scores, however, showed relatively weak enrichments or even depletions for these promoter- and TSS- associated states. For example, state PromF4, which had over 30 fold enrichment for non-coding variants prioritized by four different scores, had a 5-fold depletion for those prioritized by fitCons (**Fig. 6C**). Similarly, state TSS1 was in the top five most enriched states with bases prioritized by 10 scores (~ 5-62 folds), including the aforementioned seven scores, yet was depleted with prioritized variants by fitCons

(~ 1.2 fold depletion) (**Fig. 6C**). Enhancer states EnhA2-3,17 were among the states in the top five most enriched for FATHMM, GERP++, LINSIGHT, PhastCons, and PhyloP prioritized non-coding variants. These states also showed consistent enrichments with variants prioritized by Eigen, funSeq2, CADD, and REMM, though those scores showed even stronger relative enrichments for promoter states. In contrast, FIRE, DANN and CDS were depleted for prioritized variants in all these enhancer states, and Eigen_PC showed both enrichments and depletions (**Fig. 6C**). FIRE and fitCons showed strong enrichment for exon states (TxEx1-3), which are associated with coding regions, even though coding bases were excluded in this analysis (**Fig. 6C**). FATHMM had the greatest relative enrichment for the primary DNase state associated with CTCF cell type-specific chromatin states (DNase1) (~10 fold), and was the only score for which this state was among the top five most enriched states (**Fig. 6C, Supp. Fig. 28**).

We conducted similar analyses based on top 5% and 10% prioritized non-coding variants and observed relatively similar patterns of enrichments, though there did exist some differences at these thresholds (**Supp. Fig. 28, 30-31**). One difference was that alignment artifact associated states GapArtf2-3 were among the top two states most enriched with top 5% and 10% non-coding bases prioritized by FATHMM (**Supp. Fig. 28**). In addition, we analyzed top 1%, 5%, and 10% prioritized variants genome-wide from the 12 scores that were defined genome-wide (**Methods**). Compared to the non-coding analysis, we saw a larger number of scores that have exon-associated transcription states (TxEx1-TxEx4) among the top five enriched states with top 1% variants genome-wide, while we saw no enhancer state among the top five enriched states with top 1% variants by any score and only one enhancer state among the top five by one score (GERP++) for top 5% and 10% variants (**Supp. Fig. 32**).

We verified that the full-stack annotation showed the highest AUROC in recovering the top 1% non-coding variants compared to all 18-state cell-type-specific annotations for all 14 scores (**Supp. Fig. 33**). Compared to all 100-state cell-type-specific annotations, the full-stack model showed the highest AUROC for 13 out of 14 scores in all 127 cell types (**Supp. Fig. 33**).

Full-stack states show distinct enrichments and depletions for human genetic variation

We next analyzed full-stack states for their enrichment with human genetic sequence variation. We calculated enrichments of full-stack states with genetic variants sequenced in 15,708 genomes from unrelated individuals in the GNOMAD database stratified by minor allele frequencies (MAFs) [47]. Across eleven ranges of MAFs, the state enrichments ranged from a 2-fold enrichment to a 4-fold depletion (**Supp. Fig. 34**). As expected, the state associated with assembly gaps (GapArtf1) is most depleted with variants, regardless of the MAF range. At the other extreme, state Acet1, which is associated with simple repeats, is the most enriched state with variants for all ten minor allele frequency (MAF) ranges that are greater than 0.0001, with fold enrichments between 1.8 and 2.0 (**Supp. Fig. 34**). We verified that the high enrichment for state Acet1 was not specific to GNOMAD's calling of variants as it had a 2.0 fold enriched with common variants from dbSNP (**Methods**) (**Supp. Fig. 34**). TSS and promoters associated states, PromF4 and TSS1-2, were maximally enriched for variants in the lowest range of MAF ($0 < \text{MAF} \leq 0.0001$), 1.5-1.7 fold. The enrichment of variants for these states decreased as the MAF ranges increased, falling to 0.8-1.2 fold for variants of the highest range of MAF (0.4-0.5) (**Supp. Fig. 34**). The high enrichment for states PromF4 and TSS1-2 for rare variants is consistent with these states having high enrichment for CpG islands (75-100 fold) (**Fig. 3A**) and the high mutation rate for CG dinucleotides [48]. We observed a similar though weaker pattern of decreasing enrichments for increasing MAF for other states associated with transcriptional activities, enhancers, DNase, or promoters (**Supp. Fig. 26**). This pattern was not observed in most states from other groups such as heterochromatin, polycomb repressed, quiescent, and acetylations only (**Supp. Fig. 26**).

To better identify states with a depletion of common variants that are more likely due to selection, we ranked states based on their ratios of enrichments for the rarest variants ($\text{MAF} < 0.0001$) relative to the most common variants (MAF 0.4-0.5) (**Fig. 6D**). The states with the highest ratio included a number of flanking promoter (PromF3-4) and exon-transcription states (TxEx1,2,4) that were also associated with strong sequence conservation across species (**Fig. 6D, Fig. 3B**). These results are consistent with previous analyses supporting a depletion of common human genetic variation in evolutionary conserved regions [49]. States associated with assembly gaps and alignment artifacts (GapArtf1-3), quiescent (Quies3), or

acetylations and simple repeats (Acet1) were most depleted for rare variants relative to the common variant enrichment (**Fig. 6D**).

Full-stack states show enrichment for phenotype-associated genetic variants

We next analyzed the relationship between the full-stack states and phenotypic associated genetic variants. We first evaluated the enrichment of the full-stack state for variants curated into the Genome-wide Association Study (GWAS) catalog relative to a background of common variation [50] (**Methods**). This revealed six states with at least a two-fold enrichment (**Supp. Fig. 35**). Four of these states, TxEx1-2,4 and TxEnh4, were all transcription associated states that are ≥ 10 -fold enriched with coding sequences and ≥ 11 fold for ConsHMM state 1, associated with the most constraint in a sequence alignment of 100 vertebrates (**Fig. 3B**). This observation is consistent with previous results that GWAS catalog variants show enrichments for coding sequence and sequence constrained bases [32,49,51]. The other two states with greater than two-fold enrichment for GWAS catalog variants relative to common variants were two promoter states, PromF2-3 (**Supp. Fig. 35**). On the other hand, four states were more than two-fold depleted for GWAS catalog variants, and were associated with artifacts (GapArtf2-3), or quiescent and polycomb repressed states with weak signals of H3K9me3 (Quies5) or H3K27me3 (ReprPC8) (**Supp. Fig. 35**).

We also analyzed the full-stack state enrichments for fine-mapped variants previously generated from a large collection of GWAS studies from the UK Biobank database and other public databases [52]. Specifically, we considered separately the fine mapped variants from two fine-mapping methods, CAVIAR [53] and FINEMAP [54], for 3052 traits. For each method and trait, we identified the single variants that had the greatest probability of being causal at a set of distinct loci, and computed the enrichment of these variants for the full-stack states relative to a background of common variants (**Methods**).

Fold enrichment results of full-stack states for the most likely causal variants were highly consistent between fine-mapping methods (FINEMAP and CAVIAR) (**Supp. Fig. 36**). The ten states maximally enriched with fine-mapped variants relative to common variants, which were the same states by both methods, included five states associated with flanking and bivalent promoter activities (PromF2-5,

BivProm4), an enhancer state in blood and thymus (EnhA9) and an enhancer state in most other cell types except blood (EnhA1), and three highly conserved transcription-associated states (TxEnh4,6, TxEx4) (**Fig. 6E**). Notably, five of 10 states maximally enriched with fine-mapped variants, PromF2-5, BivProm4, were associated with promoter regions and also among the 19 states most enriched with top 1% prioritized variants by at least two of the 14 different variant prioritization scores (**Fig. 6E, C**). These results show that there are agreements in the types of chromatin states preferentially overlapped by phenotype-associated fine mapped variants and variants predicted to have greater effects based on variant prioritization scores. We also confirmed that the full-stack model consistently resulted in higher AUROC in predicting locations of fine-mapped variants within a background of common variants, compared to the 18-state and 100-state cell-type-specific annotations in all cell types (**Supp. Fig. 37-38**).

Full-stack states show enrichments for cancer-associated variants

In addition to investigating germline variants, we also investigated the enrichment of full-stack states for somatic variants identified from whole genome sequencing of cancer samples. We analyzed data of variants from four cancer types that have the largest number of somatic variants in the COSMIC database [55]: liver, breast, pancreas and haematopoietic_and_lymphoid_tissue (**Methods**). Sixteen states were among the top 10 most enriched with at least one type of cancer's associated variants (1.2-1.4 fold in breast cancer, 1.2-5.6 fold in lymphoid cancer, 1.2-5.4 in liver cancer, 1.4-4.2 in pancreas cancer) (**Fig. 6F**). Among these states, 15 states showed higher signals of H3K9me3 compared to most other chromatin marks, including seven states in heterochromatin group (HET1-2, 4-7,9), four states in quiescent group with weak emissions of H3K9me3 (Ques 1-2,4-5), one state in the polycomb repressed group with weak signals of H3K9me3 and H3K27me3 (ReprPC8), one state in the acetylation group with signals of H3K9me3 and various acetylation marks (Acet1), two artifact-associated states with higher signals of H3K9me3 and DNase relative to other marks (GapArtf2-3) (**Fig. 6G**). These results are consistent with previous findings on an association of H3K9me3 and somatic cancer-associated variants [56,57]. Acet1 was also the state most enriched with simple repeats, dbSNP 151 common variants, and variants of ten ranges of MAF from

GNOMAD (**Fig. 5C, Supp. Fig. 34**). Notably, the GapArtf2-3 states, associated with satellite repeat enrichments (**Fig. 5C, Supp. Fig. 20**), were the top two most enriched states with somatic variants associated with liver, pancreas and haematopoietic and lymphoid tissue cancers with 2.0-5.6 enrichment fold (**Fig. 6F, Supp. Fig. 39**). We note that the association between the full-stack annotations and presence of cancer variants is stronger than for the 18-state and 100-state cell-type-specific chromatin state annotations for all four cancer types, as evidenced by the higher AUROC of the full-stack annotation at predicting somatic variants (**Supp. Fig. 40-41**).

Discussion

We demonstrated a large-scale application of the stacked modeling approach of ChromHMM using over a thousand epigenomic datasets to annotate the human genome. In the datasets, 32 chromatin marks and 127 reference epigenomes were represented. We note that even though not every chromatin mark was profiled in every reference epigenome we were still able to directly apply the stacked modeling to such data. We conducted extensive enrichment analyses of the states with various other genomic annotations and datasets including gene features, genetic variation, repetitive elements, comparative genomic annotations, and bases prioritized by different variant prioritization scores. These analyses highlighted diverse enrichment patterns of the states. Using these enrichments along with the model parameters, we provided a detailed characterization of each of the 100 states in the model.

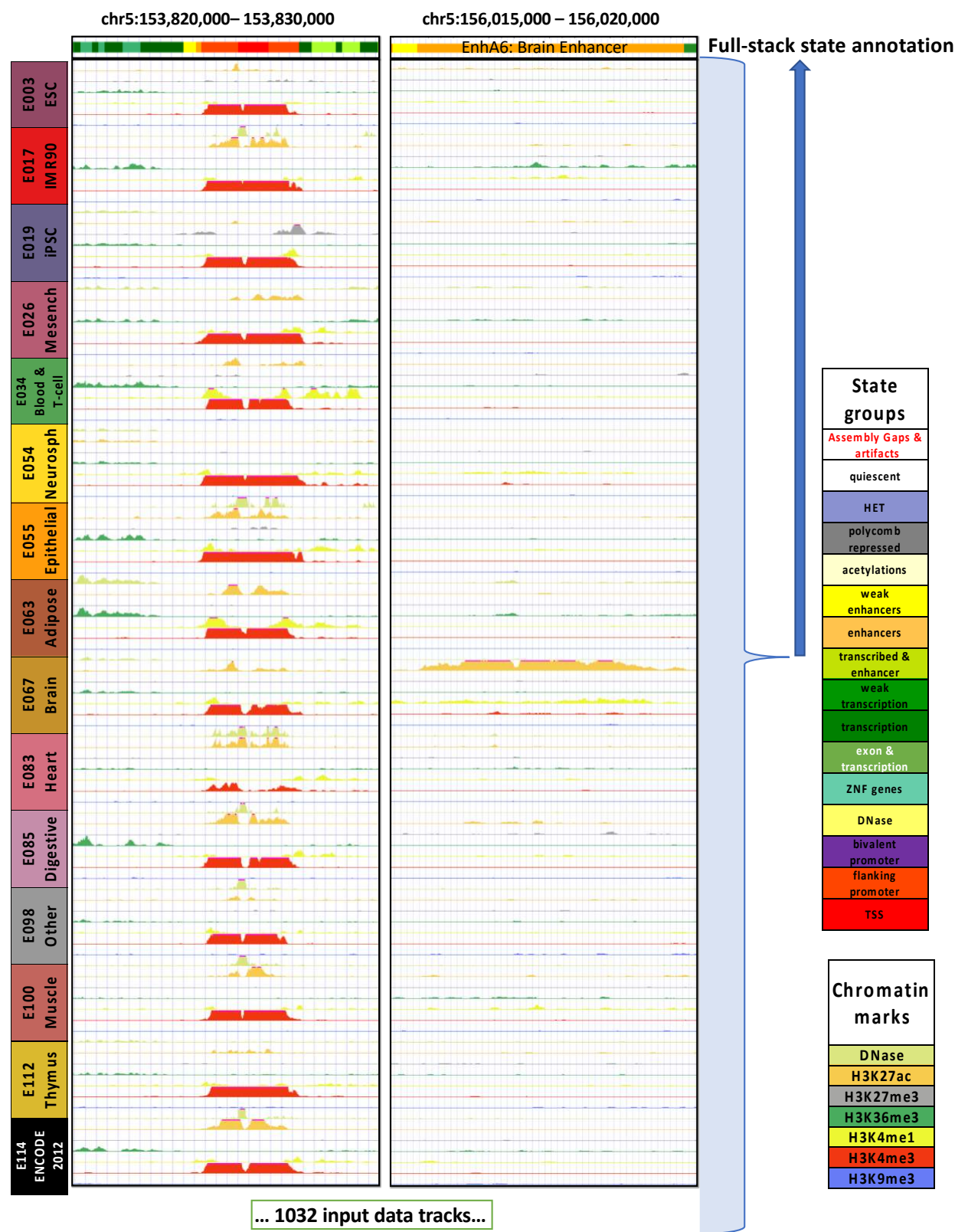
We grouped these 100 states into 16 groups that included promoters, enhancers, transcribed regions, polycomb repressed regions, zinc finger genes among others. We also highlighted important distinctions among states within the groups. In many cases, identifying these distinctions was enabled by the full-stack modeling using data from multiple cell types for genome annotation. For example, we identified enhancer and repressive states that were active in different subsets of cell types. We also highlighted how different states in some of the groups such as those associated with transcribed and ZNF genes showed distinct enrichments for conservation states. Overall, the full-stack model showed enrichment patterns supporting observations held for cell-type-specific annotations, yet it provided more detailed

stratification of genomic regions into chromatin states with heterogeneous associations with other genomic information.

The full-stack modeling has advantages to commonly used cell-type-specific chromatin state annotations in several respects. First, the full-stack model is not specific to one cell or tissue type and thus is able to provide a unified view of all the data and directly uncover states that correspond to constitutive or cell-type-specific activities. Second, the full-stack annotation consistently showed better recovery of various genomic features compared to cell-type-specific annotations. This improvement is expected since full-stack models can leverage information from multiple cell types for genome annotations. Third, in cases where it is not desirable to focus on only one specific cell or tissue for analysis, the full-stack modeling can bypass the need to pick one such cell or tissue type or to consider a large number of different cell-type-specific chromatin state annotations simultaneously. Such cases may arise when studying other genomic information that is not inherently cell-type-specific such as genome variation and sequence conservation.

However, we emphasize that the stacked modeling approach should be considered a complement to and not a replacement of the cell-type-specific annotations, which have their own advantages. Cell-type-specific annotations may be preferable when one is interested in a specific cell type or in directly comparing the chromatin state maps among individual cell types. Additionally, the cell-type-specific chromatin states have fewer parameters and thus can be easier to interpret relative to stacked model states.

We expect many applications of the full-stack annotations that we generated here. The full-stack annotation can be used as a resource to interpret genetic variation. A possible avenue for future work is to incorporate the full-stack annotation into scoring methods to better predict genetic variants' phenotypic influences. Future work could apply the stacked modeling approach to even larger sets of data that are accumulating in human as well as large datasets in key model organisms such as mouse. This work provides a new annotation resource for studying the human genome, non-coding genetic variants, and their association with diseases.



490

Figure 1: Illustration of full-stack modeling annotations. The figure illustrates the full-stack modeling at two loci. The top track shows chromatin state annotations from the full-stack modeling colored based on the legend at right. Below it are signal tracks for a subset of the 1032 input datasets. Data from seven (DNase I hypersensitivity, H3K27me3, H3K36me3, H3K4me1, H3K4me2, H3K4me3, and H3K9me3) of the 32 chromatin marks are shown, colored based on the legend at right. These data are from 15 of the 127 reference epigenomes each representing different cell and tissue groups. The loci on left highlights a genomic region for which a portion is annotated as constitutive promoter states (TSS1-2). The loci on right panel highlights a region for which a portion is annotated as a brain enhancer state (EnhA6), which has high signals of H3K27ac in reference epigenomes of the group Brain.

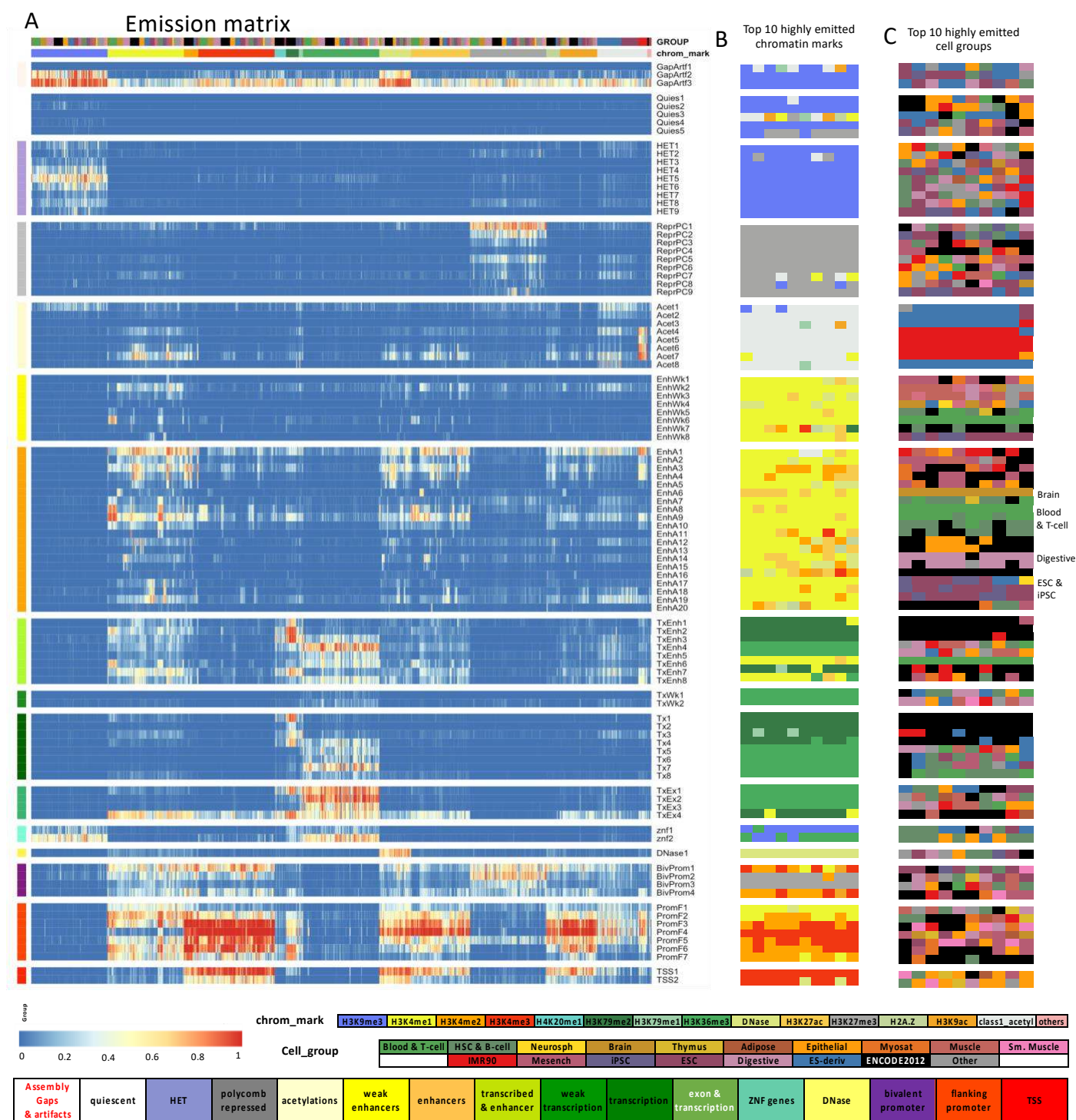


Figure 2: Full-stack state emission parameters. (A) Each of the 100 rows in the heatmap corresponds to a full-stack state. Each of the 1032 columns corresponds to one experiment. For each state and each experiment, the heatmap gives the probability within the state of observing a binary present call for the experiment's signal. Above the heatmap there are two rows, one indicating the cell or tissue type of the experiment and the other indicating the chromatin mark. The corresponding color legends are shown towards the bottom. The states are displayed in 16 groups with white space between each group. The states were grouped based on biological interpretations indicated by the color legend at the bottom. Full characterization of states is available in **Supplementary Data**. The model's transition parameters between states can be found in **Supp. Fig. 6**. Columns are ordered such that experiments profiling the same chromatin marks are next to each other.

(B) Each row corresponds to a full-stack state as ordered in (A). The columns correspond to the top 10 experiments with the highest emission value for each state, in order of decreasing ranks, colored by their associated chromatin marks as in (A).

(C) Similar to (B), but experiments are colored by the associated cell or tissue type group. We noted on the right the cell or tissue groups of some cell-type-specific enhancer states.

state	1	2	3	4	5	6	7	8	9	10	11	12	13	14	15	16	17	18	19	20	21	22	23	24	25	26	27	28	29	30	31	32	33	34	35	36	37	38	39	40	41	42	43	44	45	46	47	48	49	50	51	52	53	54	55	56	57	58	59	60	61	62	63	64	65	66	67	68	69	70	71	72	73	74	75	76	77	78	79	80	81	82	83	84	85	86	87	88	89	90	91	92	93	94	95	96	97	98	99	100
state	1	2	3	4	5	6	7	8	9	10	11	12	13	14	15	16	17	18	19	20	21	22	23	24	25	26	27	28	29	30	31	32	33	34	35	36	37	38	39	40	41	42	43	44	45	46	47	48	49	50	51	52	53	54	55	56	57	58	59	60	61	62	63	64	65	66	67	68	69	70	71	72	73	74	75	76	77	78	79	80	81	82	83	84	85	86	87	88	89	90	91	92	93	94	95	96	97	98	99	100
state	1	2	3	4	5	6	7	8	9	10	11	12	13	14	15	16	17	18	19	20	21	22	23	24	25	26	27	28	29	30	31	32	33	34	35	36	37	38	39	40	41	42	43	44	45	46	47	48	49	50	51	52	53	54	55	56	57	58	59	60	61	62	63	64	65	66	67	68	69	70	71	72	73	74	75	76	77	78	79	80	81	82	83	84	85	86	87	88	89	90	91	92	93	94	95	96	97	98	99	100
state	1	2	3	4	5	6	7	8	9	10	11	12	13	14	15	16	17	18	19	20	21	22	23	24	25	26	27	28	29	30	31	32	33	34	35	36	37	38	39	40	41	42	43	44	45	46	47	48	49	50	51	52	53	54	55	56	57	58	59	60	61	62	63	64	65	66	67	68	69	70	71	72	73	74	75	76	77	78	79	80	81	82	83	84	85	86	87	88	89	90	91	92	93	94	95	96	97	98	99	100
state	1	2	3	4	5	6	7	8	9	10	11	12	13	14	15	16	17	18	19	20	21	22	23	24	25	26	27	28	29	30	31	32	33	34	35	36	37	38	39	40	41	42	43	44	45	46	47	48	49	50	51	52	53	54	55	56	57	58	59	60	61	62	63	64	65	66	67	68	69	70	71	72	73	74	75	76	77	78	79	80	81	82	83	84	85	86	87	88	89	90	91	92	93	94	95	96	97	98	99	100
state	1	2	3	4	5	6	7	8	9	10	11	12	13	14	15	16	17	18	19	20	21	22	23	24	25	26	27	28	29	30	31	32	33	34	35	36	37	38	39	40	41	42	43	44	45	46	47	48	49	50	51	52	53	54	55	56	57	58	59	60	61	62	63	64	65	66	67	68	69	70	71	72	73	74	75	76	77	78	79	80	81	82	83	84																

[illegible]

D

enrichments

enrichment

posnt

TxEx4 (TES enriched)

TxEnh4

E

enrichment

TS51

PromF4

TS52

PromF6

PromF3

nucleotide

Orange	High align and match frequencies for a few primates
Blue	High align and match for mammals, but missing notable subsets
Green	High align and match frequencies for primates
Grey	Putative artifact
Red	High align and match frequency for all vertebrates
Yellow	High align and match for mammals
Light Yellow	High align and match for mammals and some non-mammals

Gene.exp color scale

state_type

Blood & T-cell
Brain
Digestive
ENCODE2011
Epithelial
ES-deriv
ESC
Heart
HSC & B-cell
Muscle
Neurosp
Other
Thymus

state_type
Blood & T-

Figure 3: Full stack states enrichments for external genomic annotations. (A) Fold enrichments of full-stack states with external genome annotations (**Methods**). Each row corresponds to a state and each column corresponds to one external genomic annotation: CpG Islands, Exons, coding sequences, gene bodies, transcription end sites (TES), transcription start sites (TSS), TSS and 2kb surrounding regions, lamina associated domains (laminB1lads), assembly gaps, annotated ZNF genes, repeat elements and PhastCons constrained element. The color is normalized to range from minimum values (white) to maximum values (red) within each column.

(B) Each row indicates the ConsHMM state [32] that has highest enrichment fold in each full-stack state as ordered in **(A)**. Legends of the ConsHMM state groups indicated with different colors are shown below the heatmap in **(A)**.

(C) Average weighted expression of genes that overlap each full-stack state in different groups of cells (**Methods**). Each column corresponds to a cell group indicated at the bottom. Each row corresponds to a state, as ordered in **(A)**.

(D-E) Positional enrichments of full-stack states relative to annotated **(D)** transcription end sites (TES) and **(E)** transcription start sites (TSS). Positive coordinate values represent the number of bases downstream in the 5' to 3' direction of transcription, while negative values represent the number of bases upstream. Each line shows the positional enrichments in a state. Lines are colored as indicated in **(A)**.

(F) Enrichments of full-stacks states with cell-type-specific chromatin states associated with CTCF and open chromatin, but limited histone modifications in six cell types [30] (**Methods**). The six cell types are indicated along the bottom of the figure. States are displayed horizontally in the same order as **(A)**. The DNase1 state showed the strongest enrichment for the cell-type-specific chromatin states associated with CTCF and open chromatin in all six cell types.

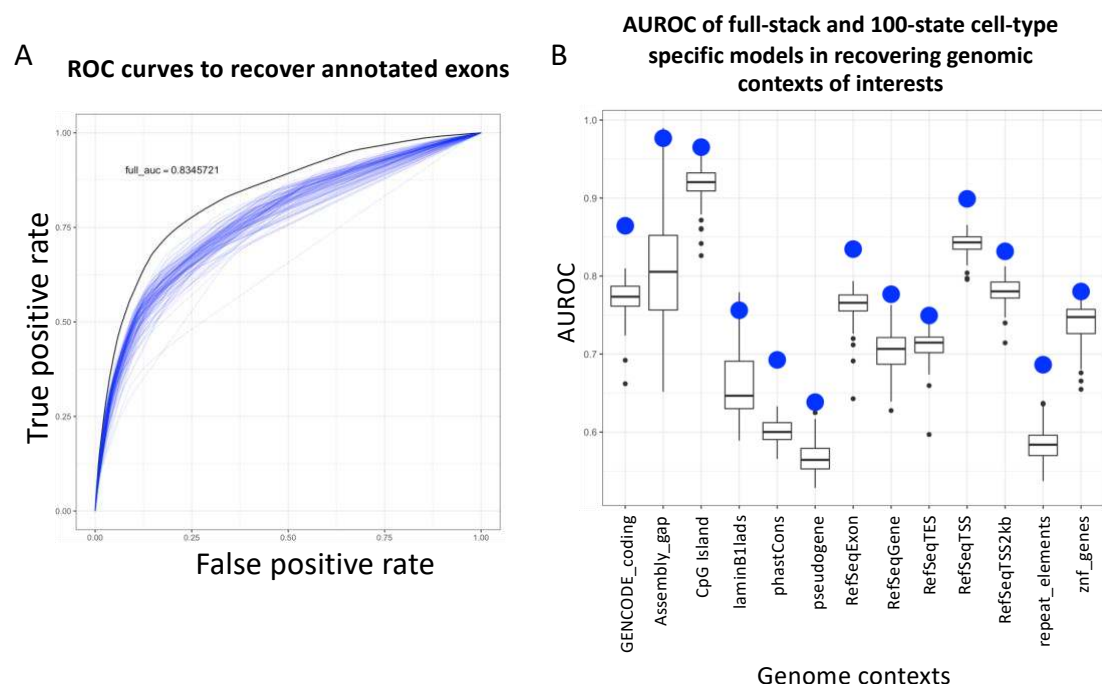


Figure 4: Full-stack annotation's recovery of external genome annotations

(A) ROC curves in recovering annotated exons by full-stack annotation (solid black line) and 127 cell-type-specific 100-state annotations (blurred blue lines). Full stack model yielded the highest AUROC (0.83).

(B) A comparison of the AUROC for full-stack annotation and cell-type-specific models for recovering positions of different external annotations. Each box plots show the range of AUROC of 100-state cell-type-specific chromatin state annotations for recovery of one external annotation and the large blue point shows the AUROC for the full-stack annotation. The external annotations in order were coding sequences, assembly gaps, CpG Islands, lamina associated domains, phastCons conserved elements, pseudogenes, exons, gene bodies, transcription end sites (TES), transcription start sites (TSS), TSS and 2kb surrounding regions, repeat elements, annotated ZNF genes. These annotations are similar to Fig. 3A. ROC curves corresponding to these AUROC values can be found in Supp. Fig. 18.

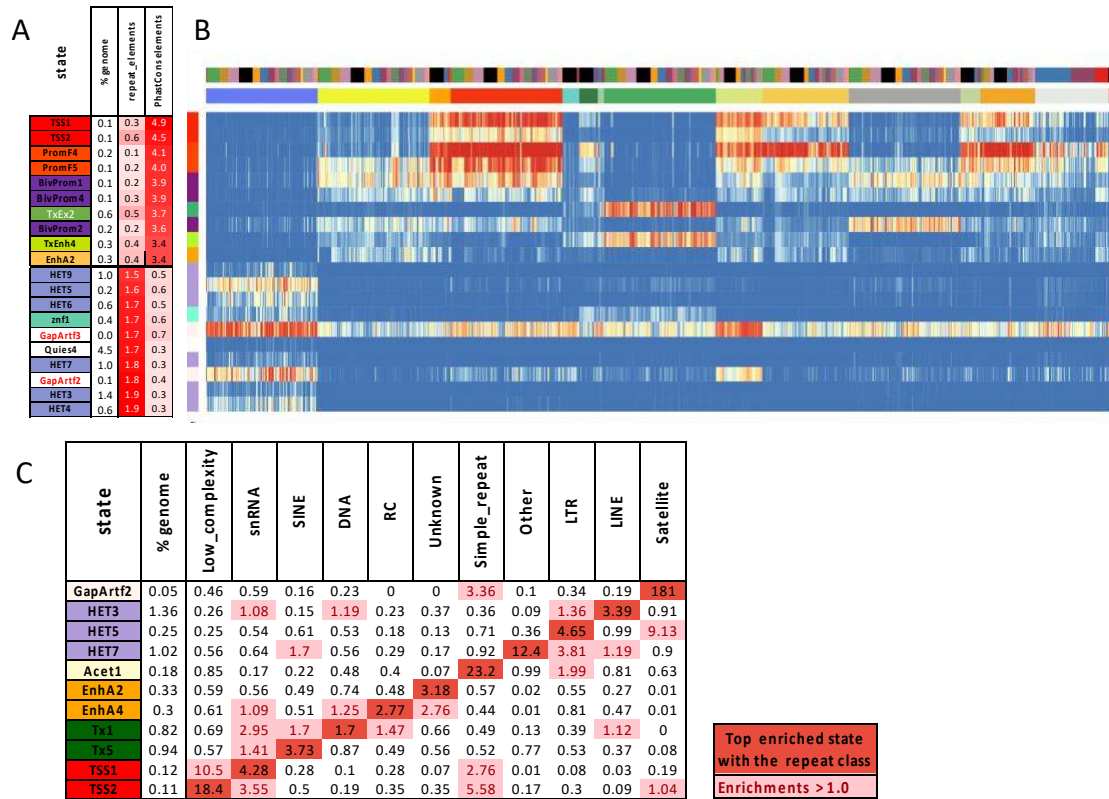


Figure 5: Full-stack states enrichments with conserved elements and repeat classes.

(A) The first ten rows show the states most enriched with PhastCons elements and concurrently least enriched with RepeatMasker repeat elements, ordered by decreasing enrichments with PhastCons elements. The bottom ten rows show the states most enriched with repeat elements and concurrently least enriched with PhastCons elements, ordered by increasing enrichments with repeat elements. The columns from left to right list the state ID, the percent of the genome that each state covers, and the fold enrichments for repeat elements and PhastCons elements.

(B) Heatmap of the state emission parameters from Fig. 2A for the subset of states highlighted in panel (A). The colors are the same in Fig. 2A.

(C) Fold enrichments of full-stack states with different repeat classes (Methods). Rows correspond to states and columns to different repeat classes. Only states that are most enriched with at least one repeat class are shown. Fold enrichment values that are maximal for a given are shown in dark red. Other fold enrichments greater than one are shaded light red.

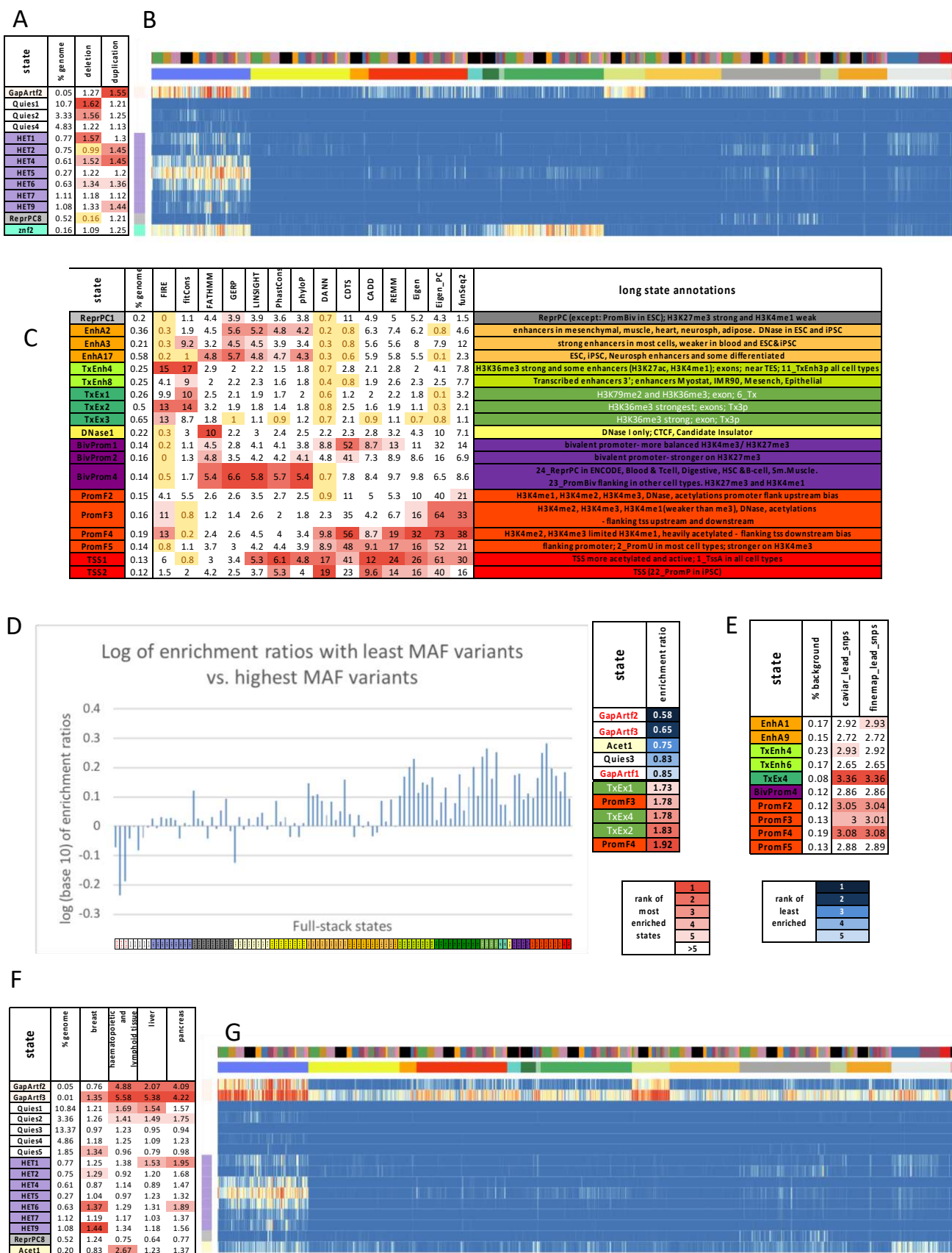


Figure 6: Full-stack states' relationship with human genetic variants.

(A) Enrichments of full-stack states with duplications and deletions from [33]. Only states that are in the top ten most enriched states are shown. Top five fold-enrichments for each class of structural variants are colored in increasing darker shades of red for higher ranked enrichments. Enrichment values below one, corresponding to depletions, are colored yellow. The columns from left to right are the state label, percent of genome the state covers, the fold enrichment for deletions, and fold enrichment for duplications.

(B) Emission probabilities corresponding to states in **(A)**. The coloring is the same as **Fig. 2A**. The figure highlights how states most associated with structural variants generally had higher emission of H3K9me3 compared to other chromatin marks.

(C) Enrichments of full-stack states with top 1% prioritized bases in the non-coding genome by 14 variant prioritization scores previously analyzed [32]. Only states that are among the top five most enriched states by at least one score are shown. The top five enrichment values for each score are colored in increasing darker shades of red for higher ranked enrichment values. Enrichment values below one, corresponding to depletions, are colored in yellow. The columns from left to right are the state label, percent of the genome covered, the 14 score enrichments, and a detailed description of the state.

(D) Log base 10 of ratios of states' enrichment with GNOMAD variants with the lowest MAFs (< 0.0001) vs. GNOMAD variants with the highest MAFs (0.4-0.5). States are ordered as in **Fig. 2A**. Top five states that with the highest and lowest enrichment ratios are labeled to the right.

(E) States most enriched with fine-mapped phenotypic variants against the background of common variants. Fine-mapped phenotypic variants were identified by either CAVIAR [53] or FINEMAP [54] (**Methods**).

(F) State enrichments with somatic mutations associated with four cancer types in the non-coding genome. Only states that are among the ten most enriched with variants from at least one cancer type are shown. States in the top five are colored according to their ranks. The top five enrichment values for each cancer type are colored in increasing darker shades of red for higher ranked enrichment values. The columns are the state label, the percent of the genome the state covers, and the fold enrichments of variants from breast, haematopoietic and lymphoid, liver, and pancreas cancer types.

(G) Emission probabilities corresponding to states in (G), as subsetting from **Fig. 2A**. The coloring is the same as **Fig. 2A**. The figure highlights how states with the greatest enrichments for cancer-associated variants tend to have higher emission probabilities for H3K9me3 compared to other chromatin marks.

Methods

Input data and processing

We obtained coordinates of reads aligned to Human hg19 in .tagAlign format for the consolidated epigenomes as processed by the Roadmap Epigenomics Consortium from <https://egg2.wustl.edu/roadmap/data/byFileType/alignments/consolidated/>. In total we obtained data for 1032 experiments and their corresponding input control data. The experiments correspond to 127 reference epigenomes, 111 of which were generated by the Roadmap Epigenomics Consortium and 16 were generated by the ENCODE Consortium. Of the 1032 experiments, 979 were of ChIP-seq data targeting 31 different epigenetic marks and 53 were of DNase-seq (**Sup Fig. 2**). For each of the 127 reference epigenomes there was a single ChIP-seq input control experiment. For the 53 reference epigenomes that had a DNase-seq experiment available there was an additional DNase control file.

We next binarized the data at 200 base pair resolution using the BinarizeBed command of ChromHMM (v.1.18). To apply BinarizeBed in stacked mode we generated a cell_mark_file input table for ChromHMM with four tab-delimited columns. The first column had the word ‘genome’ for all datasets, the second column contained entries of the form ‘<EID>-<mark>’ where ‘EID’ is the epigenome ID and ‘mark’ is the mark name, the third column specifies the name of the corresponding file with aligned reads, and the fourth column is the name of the file with the corresponding control reads. Each row in the table corresponds to one of the 1032 experiments.

In order to reduce the memory and time needed to execute BinarizeBed on a large number of datasets, we split the cell_mark_file table into 104 smaller tables with each table having at most 10 entries corresponding to at most 10 datasets to be processed. This was done with a custom script, but the same functionality has been included with the ‘-splitcols’ and ‘-k’ flags of BinarizedBed in ChromHMM v1.22. We then ran BinarizeBed in parallel for each of these smaller cell_mark_file tables and generated output into separate sub-directories. We ran BinarizeBed with the option ‘-gzip’ which generates gzipped files.

To merge data from the 104 subdirectories from the previous step into files containing binarized data of all experiments, we ran the command ‘MergeBinary’, which we added in v1.18 of ChromHMM. We ran the command with the options ‘-gzip -splitrows’. The ‘-splitrows’ option generates multiple files of merged binarized data for each chromosome, where, under the default settings that we used, each file contains data for a genomic region of at most 1MB. Splitting each chromosome into smaller regions allows the model learning step of ChromHMM to scale in terms of memory and time to the large number of input data tracks (i.e. features) that we were using. We used chr1-22, chrX, chrY, and chrM in the binarization and model learning.

Training full-stack model and generating genome-wide state annotations

We learned the full-stack chromatin state model for the 1032 datasets using the LearnModel command of ChromHMM (v1.18). This version of ChromHMM includes several options that we added to improve the scalability when training with large numbers of features. One of these features was to randomly sample different segments of the genome for training during each iteration, instead of training on the full genome. This sampling strategy was previously used by ConsHMM [32], which was built on top of ChromHMM. To learn the full-stack model with input data processed as outlined above, we used ChromHMM’s LearnModel command with the options ‘-splitrows -holdcolumnorder -pseudo -many -p 6 -n 300 -d -1 -lowmem -gzip’.

The ‘-splitrows’ flag informs ChromHMM that binarized data for a chromosome is split into multiple files, which reduces the memory requirements and allows ChromHMM to select a subset of the genome to train on for each iteration. The ‘-holdcolumnorder’ flag prevents ChromHMM from reordering the columns of the output emission matrix, which saves time when there is a large number of features.

The ‘-pseudo’ flag specifies that in each update of model parameters, ChromHMM adds a pseudo count of one to the numbers of observations of transition between each pair of states, presence and absence of each mark from each state, and initial state assignments of the training chromatin state sequence. This

prevents model parameters from being set to zero, which is needed for numerical stability when some features are sparse and ChromHMM does not train on the full genome in each iteration.

The ‘-many’ flag specifies ChromHMM to use an alternative procedure for calculating the state posterior probabilities that is more numerically stable when there are a large number of features. The procedure is designed to prevent all states from having zero posterior probability at any genomic position, which can happen due to the limits of floating-point precision. The procedure does this by leveraging the observation that only the relative product of emission probabilities across states are needed at each position to determine the posterior probabilities. Specifically, for each position, the procedure initializes the product of emission probabilities for all features, i.e. the emission product, from each state to one. For each feature, the procedure then multiplies the current emission products from each state by the emission probability of the feature in the state, and divides all the resulting products by their maximum to obtain updated emission products. We iteratively repeat these steps of multiplication and normalization until all features have been included into the calculation of relative emission products across states.

The ‘-p 6’ flag specifies to ChromHMM to train the model in parallel using 6 processors. The ‘-n 300’ flag specifies to ChromHMM to randomly pick 300 files of binarized data, corresponding to 300 regions of 1 MB (or less if the last segment of the chromosome was selected) for training in each iteration. The ‘-d -1’ option has ChromHMM not require an evaluated likelihood improvement between iterations to continue training since likelihood decreases are expected as on each iteration the likelihood is evaluated on a different subset of data. The ‘-lowmem’ flag has ChromHMM reduce main memory usage by not storing in main memory all the input data and instead re-loading from disk when needed.

Choice of number of states

We trained full-stack models with 20, 40, 60, 80, 100 and 120 states, using the data and procedure outlined above. We then quantitatively compared the chromatin state annotations from these models in terms of their power to predict locations of various other genomic annotations not used in the model training: Exon, Gene Body, TSS, TSS2kb, CpG Islands, TES, laminB1lads elements (listed in section

External Annotation Sources section). Specifically, we evaluated the predictive power using the AUROCs that are calculated as described in a subsection below. Across different genomic contexts, as the number of full-stack states increased, the AUROC increased, but the marginal increase was smaller as the number of states increased (**Supp. Fig. 3**). To balance the additional information available in models with increased number of states, while keeping the number of states manageable for interpretation and downstream analysis, we choose to focus on a model with 100 states. We note that this choice is greater than previously used for cell-type-specific chromatin state models [3,16,21], reflecting the additional information available for genome annotation based on the large number of datasets spanning many cell types that we are using.

Lifting chromatin state annotations to hg38

The chromatin state annotation resulted from stacked modeling was in hg19. In order to obtain the annotations for hg38, we first wrote the chromatin state map hg19 in .bed format such that each line corresponds to a genomic region of 200bp. We then used liftOver tools downloaded from UCSC utilities to generate the chromatin state annotation in hg38. In total, there are 1,186,379 200-bp segments that were not mapped from hg19 to hg38.

Summary sets of experiments

To construct a summary visualization of the emission parameters with a reduced set of features that approximate the annotation from the full model, we applied a greedy search over the 1032 input datasets as described in **Supplementary Methods**. We applied this procedure to reduce the 1032 input datasets to 80 summary datasets.

Identifying states with differential association of marks for individual tissue groups

For each state, we tested for combinations of the 8 most profiled marks, and 19 tissue groups previously defined [16], whether the emission probabilities of features associated with one chromatin mark

and in one tissue group was significantly greater than those of features associated with the same mark and not in the tissue group. The eight marks that we tested were H3K9me3, H3K4me1, H3K4me3, H3K27me3, H3K36me3, H3K27ac, H3K9ac, and DNase. H3K27ac, H3K9ac and DNase were profiled in 98, 62 and 53 reference epigenomes, respectively, and the remaining five marks in 127 reference epigenomes. For tests involving H3K27ac, H3K9ac, and DNase, we excluded tissue groups for which there were no experiments. In total, there were 14,200 tests among 100 states, 8 chromatin marks and 19 tissue groups. For each combination of state, chromatin mark and tissue group being tested, we applied a one-sided Mann-Whitney test to test whether the emission probabilities of the state for the features associated with the tested mark in the tested tissue group are greater than those in other tissue groups. The Bonferroni-corrected p-value threshold based on a significance level of 0.05 to declare a test significant was $3.5e-6$.

Computing coefficients of variation across different tissue groups

For each state, we looked into the emission probabilities of experiments associated with six chromatin marks strongly associated with promoter and enhancer activities (DNase, H3K27ac, H3K4me1, H3K4me2, H3K4me3, H3K9ac). We grouped these experiments based on their associated chromatin mark and tissue groups, and calculated the average emission probabilities of experiments in each chromatin mark-tissue group combination. For each state and chromatin mark combination, we then calculated the coefficient of variation across different tissue groups, in terms of average emission probabilities from the previous step. For each group of states, we averaged the resulting coefficients of variation across states of the same group. The results show the average coefficients of variation of emission probabilities across different tissue groups for each state group- chromatin mark combination.

Computing fold enrichments for other annotations

All overlap enrichments for external annotations were computed using the ChromHMM OverlapEnrichment command. We used the '-b 1' flag, which specifies a binning resolution of the annotations. This '-b 1' flag is necessary when computing enrichments based on the hg38 liftOver

annotations, which no longer respects the 200bp segment coordinate intervals from hg19. Including this flag gives the same results when applied to annotations from hg19 with 200bp segments, though with extra computational costs. We also included the ‘-lowmem’ flag to specify the lower memory usage option. The ChromHMM command `OverlapEnrichment` computes fold enrichment between chromatin states and provided external annotations relative to a uniform genome-wide background distribution. More specifically, the fold enrichments are calculated as:

$$FE_{x,s} = \frac{\frac{\#SX}{\#X}}{\frac{\#S}{\#G}} = \frac{\frac{\#SX}{\#S}}{\frac{\#X}{\#G}} = \frac{\#SX \cdot \#G}{\#S \cdot \#X}$$

where

$FE_{x,s}$: fold enrichment of state s in genomic context x

$\#S$: number of genomic positions belonging to the state S

$\#X$: number of genomic positions where genomic context X is present

$\#SX$: number of genomic bins that overlap both state S and genomic context X

$\#G$: number of genomic positions in the entire genome

Enrichment with cell-type-specific ChromHMM annotations

We computed the enrichments of the full-stack states for cell-type-specific ChromHMM chromatin state annotations. For the cell-type-specific chromatin state annotations we used 25-state ChromHMM annotations of 127 reference epigenomes from the Roadmap Epigenomics project. This model was trained using the concatenated modeling approach using imputed data of 12 chromatin marks [16,22]. For each of the 100 full-stack states, we calculated the enrichment for the 25 states separately in each of the 127 reference epigenomes, resulting in 127 tables of 25 enrichment values for each of the 100 states. We summarized this information by reporting, for each of the 100 full-stack states, and 127 reference epigenomes, the cell-type-specific state among the 25 states that is maximally enriched, resulting in a 100-by-127 table. We also summarized the information by reporting for each of the 100 full-stack states and 25

cell-type-specific states, the maximum and median fold enrichments across the 127 reference epigenomes
(Supplementary Data).

Receiver operator characteristic curve analysis for predicting external annotations

To evaluate the information available in the chromatin state annotations from a chromatin state model that can help predict locations of an external genomic annotation, we computed the Receiver Operator Characteristic (ROC). To do this, we first divided the genome into 200bp bins, and randomly partitioned 50% of the bins for training and the remaining 50% for testing. For a target external genome annotation, we computed the enrichment of such annotation with each chromatin state on the training data. We then ranked states in decreasing order of enrichments for the target annotation. We used this ranking of states to iteratively add genomic bases assigned to the added state to our predictions of bases overlapping the target annotation in the testing dataset. Based on the overlap of the predictions and the target annotation at each iteration, we plotted ROC curves and summarized the information by computing area under the ROC curves (AUROC).

Cell-type-specific ChromHMM annotations for comparing predictive information

We compared the full-stack model to two sets of cell-type-specific annotations in terms of their ability to predict external annotations. One set of cell-type-specific annotations was the 18-state ChromHMM from Roadmap Epigenomic Project [16], which was trained using observed data for six chromatin marks: H3K4me1, H3K4me3, H3K9me3, H3K27ac, H3K27me3 and H3K36me3, using the concatenated approach.

The second set of cell-type-specific ChromHMM annotations were annotations we generated here to have a more stringent comparison. We partitioned the 1032 datasets we used to learn the full-stack model into 127 subsets based on their associated reference epigenome. For each of these 127 subsets, we applied ChromHMM to learn a cell-type-specific model with 100 states. We learned these models with the same procedure as described above for the full-stack model, with the exception of using the ‘-init random’ flag

to randomly initialize models' parameters. This flag was necessary since for some reference epigenomes, the number of specified states (100) was greater than the number of combinations of input datasets, which is the maximum number of states supported by ChromHMM default initialization. We specified the number of states as 100 in these cell-type-specific models to control for the number of states in comparing with the full-stack model. However, we note that due to the large number of states relative to the input tracks, some of these models ended up having fewer than 100 states being assigned to positions in the genome.

Computing fine-mapped variant enrichment

To compute enrichment of full-stack states for phenotypically associated fine-mapped variants, we downloaded data on fine-mapped variants for 3052 traits from CAUSALdb [52]. Specifically we obtained posterior probabilities of variants being causal based on two fine-mapping methods, FINEMAP [54] and CAVIAR [53], which do not use epigenomic annotations as part of the fine mapping procedure. For each method and trait combination, we separately partitioned the provided set of potential causal variants into distinct loci. To form the distinct loci, we merged neighboring variants into the same loci until there was at least 1MB-gap between the two closest variants from different loci. Separately for each fine-mapping method, trait, and locus combination, we selected the single variant with the highest posterior probability of being causal. For each fine-mapping method, we took the union of variants across 3052 traits, and then calculated the fold enrichments for the union of these lead variants with stacked ChromHMM states relative to the enrichment with a background set of common variants from dbSNP build 151 (hg19). To do this, we separately computed the enrichments of both of these sets relative to a genome-wide background, and then divided the enrichment of the foreground set (lead fine-mapped variants) by the enrichment of the background set (common variants). The dbSNP variants were obtained from the UCSC genome browser.

Computing structural variant enrichments

To compute enrichment of the full-stack states for structural variant enrichments, we obtained data of structural variants from [33]. We used the B38 call set, which was in hg38 and used for the analysis

presented in [33]. We filtered out structural variants that did not pass the quality control criteria of [33]. We then separately considered structural variants annotated as either a deletion or a duplication, for which there were, 112,328 and 28,962 sites respectively.

Since the structural variants were defined in hg38, we computed their enrichment for ChromHMM state annotations in full-stack and cell-type-specific models that were lifted over from hg19 to hg38, following the procedure outlined above. Next, we followed the enrichment analysis procedure outlined above to compare full-stack vs. cell-type-specific chromatin state segmentations' power in recovering structural variants.

To compare the power of full-stack state annotations vs. cell-type-specific state annotation frequency, we utilized 15-state genome-wide chromatin state data for 127 cell types (reference epigenomes) from Roadmap Epigenomics Consortium. We followed the analysis outlined in [33], for each of the 15 ChromHMM states, we annotated genomic positions based on the number of cell types in which the state is present (ranging from 0 to 127), resulting in 15 state-specific models' annotations. We then applied the procedure above to compare the predictive power of different models' annotations against the full-stack annotation. For the state-specific models, the enrichment values are calculated for structural variants and number of cell types that a ChromHMM state is assigned to.

Computing enrichments with cancer-associated variants

We obtained data of somatic mutations associated with different types of cancer from COSMIC non-coding variants dataset v.88 in hg38 [55]. We selected from this dataset variants that were from whole-genome sequencing. We filtered out variants that overlap with any of the following: the hg38 black-listed regions from the ENCODE Data Analysis Center (DAC) [58], hg38 dbSNP (v151) set of common variants from the UCSC genome browser database, or regions annotated as coding sequence ('CDS') based on GENCODE v.30 hg38 [59] gene annotations. We decided to restrict this analysis to the four cancer types with the most number of variants present in the dataset in hg38: liver (1,351,417), pancreas (500,930), haematopoietic and lymphoid tissue (354,501), and breast (323,751), we then lifted over these sets of

variants from hg38 to hg19, resulting in 1,351,159, 500,798, 354,351, and 323,685, variants respectively. To obtain a background set of genomic locations for the enrichment analysis, we filtered from the genome the same set of hg38 annotations of black-listed regions, common variants, and coding sequences. We then lifted over these remaining positions from hg38 to hg19 to obtain the background. We calculated the enrichment of chromatin states with cancer-associated variants by first calculating the enrichment values of chromatin states with filtered variants associated with each of the four cancer types, and the enrichment values with background set of genomic bases, all relative to the whole genome. We then divided the cancer-associated variant enrichment values by the background bases enrichments.

External annotations sources

The sources for external annotations for enrichments analyses, not given above, were as follows:

- CpG island annotations were those included in the ChromHMM (v1.18) and originally obtained from the UCSC genome browser.
- Annotations of exon, gene bodies, transcription start (TSS), and transcription end sites (TES), 2kb windows surrounding TSSs (TSS2kb) were RefSeq annotations included in ChromHMM (v1.18) and originally based on annotations obtained from the UCSC genome browser.
- Lamina associated domains were for human embryonic lung fibroblasts that were included in ChromHMM (1.18), which were lifted over to hg19 from hg18 positions originally provided by [60].
- Annotations of assembly gaps were obtained from the UCSC genome browser and correspond to the Gap track.
- Annotations of zinc finger (ZNF) genes correspond to coordinates of genes whose name contained 'ZNF' from GENCODE's hg19 gene annotation, v30 [59].
- Annotations of coding sequences correspond to coordinates of genes whose feature type is 'CDS' from GENCODE's hg19 gene annotation, v30 [59].

- Annotations of pseudogenes correspond to coordinates of genes whose gene type or transcript type contained ‘pseudogene’ from GENCODE’s hg19 gene annotation, v30 [59].
- Annotations of repeat elements were obtained from UCSC genome browser RepeatMasker hg19 tracks.
- Cell-type-specific ChromHMM chromatin state annotations were obtained from the Roadmap Epigenomics Consortium through <http://compbio.mit.edu/roadmap> [16]. These include data of the 15-state and 18-state models based on observed data and the 25-state chromatin model based on imputed data for 127, 98 and 127 reference epigenomes, respectively.
- CTCF- cell-type-specific chromatin states were based on the ChromHMM chromatin state annotations for six human cell types (GM12878, H1ESC, HeLa3, Hepg2, Huvec, K562) for a 25-state model from the ENCODE integrative analysis [22,30]. We extracted coordinates of region annotated to the ‘Ctcf’ and ‘CtcfO’, both associated with CTCF signal and limited histone mark signal.
- Blacklisted regions were those provided by the ENCODE Data Analysis Center (DAC) for hg19 and hg38 [58].
- ConsHMM conservation state annotations for human (hg19) were those from [32].
- Annotations of human genetic variants and their allele frequency were from GNOMAD v2.1.1 [47]. The dataset includes 229 million SNVs and 33 million indels from 15,708 genomes of unrelated individuals, which are aligned against the GRCg37/hg19 reference.
- GWAS catalog variants were obtained from the NHGRI-EBI Catalog, accessed on December 5th, 2016 [50].

Analysis of gene expression across states

To analyze the relationship between gene expression and the full-stack states, we downloaded gene expression data from the Roadmap Epigenomics Consortium [16]. Specifically, we downloaded a matrix of gene expression values, in RPKM (Reads Per Kilobase Million), for protein coding genes for 56 reference epigenomes that were among the 127 used as part of the full-stack model. In total, we obtained expression values for 19,795 Ensembl protein coding genes.

The gene expression data was obtained from (<https://egg2.wustl.edu/roadmap/data/byDataType/rna/expression/57epigenomes.exon.RPKM.pc.gz>). We also obtained the corresponding genomic coordinates for these genes from (https://egg2.wustl.edu/roadmap/data/byDataType/rna/expression/Ensembl_v65.Gencode_v10.ENSEG.gene_info). For this analysis, we filtered out genes that are not classified as protein-coding. We transformed the gene expression values by adding a pseudo-count of 1 to the raw counts in RPKM, and taking the log of the resulting values.

For each full-stack-state and 56 reference epigenomes, we calculated the average gene expression of all genes overlapping with the state, taking into account the genes' length. For each gene g we denote its length L_g and expression E_g . We let s_i denote the state assigned at the 200-bp bin i and G_i denote the set of genes overlapping the 200bp bin i . Let B_s denote the set of 200bp bins that are assigned to state s . The average normalized expression with state s then becomes:

$$avg \exp bp \text{ normalized }_s = \frac{\sum_{i \in B_s} \sum_{g \in G_i} E_g / L_g}{\sum_{i \in B_s} \sum_{g \in G_i} 1 / L_g}$$

We also calculated for each state the average and coefficient of variation of these averages across reference epigenomes. We used the BEDTools *bedtools intersect* command to obtain the chromatin state assignments for 200bp segments that totally or partially overlap with any gene. To obtain average gene expressions of a state in a cell group as presented in **Fig. 3C**, we averaged the reported bp-normalized average gene expressions of the corresponding state across cell types within the group.

We also analyzed average gene expression values for each state as a function of the position of the state annotations relative to TSS, following a procedure similar to what was used previously [3]. We first

identified a gene's outer transcription start site (TSS) based on the reported coordinates of the gene and strand in the gene annotation file noted above. For each 200bp bin that is within 25kb upstream or downstream of an annotated TSS, including those that directly overlap with an annotated TSS, we determined the assigned full-stack state at this bin, and the position of the bin relative to those TSSs. Bins directly overlapping an annotated TSS were at position 0. If the gene was on the positive strand, the segments' genomic coordinates lower than the TSSs' correspond to upstream regions at negative points (minimum value: -250000), while genomic coordinates higher than the TSSs' correspond to downstream regions at positive points (maximum value: 25000). If the gene is on the negative strand, the upstream and downstream positions are reversed. For each state and each 200-bp bin position relative to TSS, we determined the subset of genes where there is a 200bp bin annotated to that state at that position relative to their TSSs, and calculated their average expression. This produces a 100-by-251 table for one reference epigenome, corresponding to the number of full-stack states and 200-bp segments intersecting the 50kb windows surrounding genes' TSSs and one segment directly overlapping the TSSs. We then smoothened the averaged expression data spatially by applying the sliding window average algorithm with a window size of 21, i.e. each segment's smoothened gene expression is the average of data in that segment and 21 surrounding genomic segments. Data of average gene expression in the first and last 10 segments within the 50kb window are not included in the window of smoothened data. We averaged results of 56 tables corresponding to 56 reference epigenomes as the final output from this procedure.

Computing enrichment for bases prioritized by variant prioritization scores

To compute state enrichments for bases prioritized by different variant prioritization scores, we followed the approach of [32]. We obtained coordinates of bases containing prioritized variants based on 14 different methods as processed and described in [32]. The scores were Eigen and Eigen-PC version 1.1, funSeq2 version 2.1.6, and CADD v1.4, REMM, FIRE, fitCons, CDTS, LINSIGHT, FATHMM, GERP++, phastCons, phyloP and DANN [34–46]. For 12 of the 14 scores, we separately considered prioritized variants genome-wide and in non-coding regions only. Two of the variant prioritization scores, LINSIGHT

and FunSeq2 [36,38], were defined only in the non-coding regions, so these scores were only used in the non-coding region analysis. As described in [32], the regions included in the non-coding analysis were defined as the bases where both LINSIGHT and FunSeq2 provided scores, which was 90.4% of the genome. For both the non-coding and whole genome analysis we computed the enrichment for bases ranked in the top 1%, 5% or 10% using the variant prioritization scores. We note that because of ties in some scores, the score-threshold above which we classified the bases as prioritized was chosen to be as close as possible to the target percentage (1%, 5% or 10%). We also note that if there were any bases with missing values for any particular score, then that base was assigned with the minimum values of such scores.

Enrichment values for the whole genome were computed as described above with the OverlapEnrichment command from ChromHMM. For computing enrichments restricted to non-coding regions, we first calculated enrichment of the non-coding prioritized variants relative to the whole genome and the enrichment of non-coding regions as defined above relative to the whole genome. We then divided these two enrichment values to obtain the enrichment of prioritized non-coding variants within non-coding regions.

Data availability

Full-stack chromatin state annotation of the genome is available at https://github.com/ernstlab/full_stack_ChromHMM_annotations. An updated version of ChromHMM is available at <https://ernstlab.biolchem.ucla.edu/ChromHMM/>

Acknowledgements

We thank Adriana Arneson for helping us in collecting data of analyses involving prioritized variants, repeat classes and GWAS catalog variants. We acknowledge funding from US National Institute of Health (DP1DA044371, U01MH105578); US National Science Foundation (CAREER Award #1254200); Kure-IT award from Kure It cancer research, a Rose Hills Innovator Award, and the UCLA

1051 Jonsson Comprehensive Cancer Center and Eli and Edythe Broad Center of Regenerative Medicine and

1052 Stem Cell Research Ablon Scholars Program.

1053

1054 **Ethics Declarations**

1055 The authors announce no conflicts of interests.

References

1. Barski A, Cuddapah S, Cui K, Roh T-Y, Schones DE, Wang Z, et al. High-resolution profiling of histone methylations in the human genome. *Cell*. Elsevier; 2007;129:823–837.
2. Boyle AP, Davis S, Shulha HP, Meltzer P, Margulies EH, Weng Z, et al. High-resolution mapping and characterization of open chromatin across the genome. *Cell*. Elsevier; 2008;132:311–322.
3. Ernst J, Kheradpour P, Mikkelsen TS, Shores N, Ward LD, Epstein CB, et al. Mapping and analysis of chromatin state dynamics in nine human cell types. *Nature*. Nature Publishing Group; 2011;473:43–49.
4. Thurman RE, Rynes E, Humbert R, Vierstra J, Maurano MT, Haugen E, et al. The accessible chromatin landscape of the human genome. *Nature*. Nature Publishing Group; 2012;489:75–82.
5. Xie W, Schultz MD, Lister R, Hou Z, Rajagopal N, Ray P, et al. Epigenomic analysis of multilineage differentiation of human embryonic stem cells. *Cell*. Elsevier; 2013;153:1134–1148.
6. Taberlay PC, Statham AL, Kelly TK, Clark SJ, Jones PA. Reconfiguration of nucleosome-depleted regions at distal regulatory elements accompanies DNA methylation of enhancers and insulators in cancer. *Genome Res*. Cold Spring Harbor Lab; 2014;24:1421–1432.
7. Claussnitzer M, Dankel SN, Kim K-H, Quon G, Meuleman W, Haugen C, et al. FTO obesity variant circuitry and adipocyte browning in humans. *N Engl J Med*. Mass Medical Soc; 2015;373:895–907.

1076 8. Gjoneska E, Pfenning AR, Mathys H, Quon G, Kundaje A, Tsai L-H, et al. Conserved
1077 epigenomic signals in mice and humans reveal immune basis of Alzheimer’s disease. *Nature*.
1078 Nature Publishing Group; 2015;518:365–369.

1079 9. Kheradpour P, Ernst J, Melnikov A, Rogov P, Wang L, Zhang X, et al. Systematic dissection
1080 of regulatory motifs in 2000 predicted human enhancers using a massively parallel reporter
1081 assay. *Genome Res. Cold Spring Harbor Lab*; 2013;23:800–811.

1082 10. Varshney A, Scott LJ, Welch RP, Erdos MR, Chines PS, Narisu N, et al. Genetic regulatory
1083 signatures underlying islet gene expression and type 2 diabetes. *Proc Natl Acad Sci. National*
1084 *Acad Sciences*; 2017;114:2301–2306.

1085 11. Lay FD, Triche TJ, Tsai YC, Su S-F, Martin SE, Daneshmand S, et al. Reprogramming of
1086 the human intestinal epigenome by surgical tissue transposition. *Genome Res. Cold Spring*
1087 *Harbor Lab*; 2014;24:545–553.

1088 12. Lee J, Krivega I, Dale RK, Dean A. The LDB1 complex co-opts CTCF for erythroid lineage-
1089 specific long-range enhancer interactions. *Cell Rep. Elsevier*; 2017;19:2490–2502.

1090 13. Consortium EP. Identification and analysis of functional elements in 1% of the human
1091 genome by the ENCODE pilot project. *nature. Nature Publishing Group*; 2007;447:799.

1092 14. Consortium EP. An integrated encyclopedia of DNA elements in the human genome. *Nature*.
1093 *Nature Publishing Group*; 2012;489:57–74.

- 1094 15. Fernández AF, Bayón GF, Urduño RG, Toraño EG, García MG, Carella A, et al.
1095 H3K4me1 marks DNA regions hypomethylated during aging in human stem and differentiated
1096 cells. *Genome Res.* Cold Spring Harbor Lab; 2015;25:27–40.
- 1097 16. Kundaje A, Meuleman W, Ernst J, Bilenky M, Yen A, Heravi-Moussavi A, et al. Integrative
1098 analysis of 111 reference human epigenomes. *Nature.* Nature Publishing Group; 2015;518:317–
1099 330.
- 1100 17. Mikkelsen TS, Ku M, Jaffe DB, Issac B, Lieberman E, Giannoukos G, et al. Genome-wide
1101 maps of chromatin state in pluripotent and lineage-committed cells. *Nature.* Nature Publishing
1102 Group; 2007;448:553–560.
- 1103 18. Wang Q, Yu G, Ming X, Xia W, Xu X, Zhang Y, et al. Imprecise DNMT1 activity coupled
1104 with neighbor-guided correction enables robust yet flexible epigenetic inheritance. *Nat Genet.*
1105 Nature Publishing Group; 2020;52:828–839.
- 1106 19. Zhu J, Adli M, Zou JY, Verstappen G, Coyne M, Zhang X, et al. Genome-wide chromatin
1107 state transitions associated with developmental and environmental cues. *Cell.* Elsevier;
1108 2013;152:642–654.
- 1109 20. Stunnenberg HG, Abignani S, Adams D, de Almeida M, Altucci L, Amin V, et al. The
1110 International Human Epigenome Consortium: a blueprint for scientific collaboration and
1111 discovery. *Cell.* Elsevier; 2016;167:1145–1149.
- 1112 21. Ernst J, Kellis M. Discovery and characterization of chromatin states for systematic
1113 annotation of the human genome. *Nat Biotechnol.* Nature Publishing Group; 2010;28:817–825.

- 1114 22. Ernst J, Kellis M. ChromHMM: automating chromatin-state discovery and characterization.
1115 Nat Methods. Nature Publishing Group; 2012;9:215–216.
- 1116 23. Hoffman MM, Buske OJ, Wang J, Weng Z, Bilmes JA, Noble WS. Unsupervised pattern
1117 discovery in human chromatin structure through genomic segmentation. Nat Methods. Nature
1118 Publishing Group; 2012;9:473.
- 1119 24. Libbrecht MW, Rodriguez OL, Weng Z, Bilmes JA, Hoffman MM, Noble WS. A unified
1120 encyclopedia of human functional DNA elements through fully automated annotation of 164
1121 human cell types. Genome Biol. Springer; 2019;20:180.
- 1122 25. Ernst J, Kellis M. Chromatin-state discovery and genome annotation with ChromHMM. Nat
1123 Protoc. Nature Publishing Group; 2017;12:2478.
- 1124 26. Biesinger J, Wang Y, Xie X. Discovering and mapping chromatin states using a tree hidden
1125 Markov model. BMC Bioinformatics. Springer; 2013. p. S4.
- 1126 27. Zhang Y, An L, Yue F, Hardison RC. Jointly characterizing epigenetic dynamics across
1127 multiple human cell types. Nucleic Acids Res. Oxford University Press; 2016;44:6721–6731.
- 1128 28. Chronis C, Fiziev P, Papp B, Butz S, Bonora G, Sabri S, et al. Cooperative binding of
1129 transcription factors orchestrates reprogramming. Cell. Elsevier; 2017;168:442–459.
- 1130 29. Mortazavi A, Pepke S, Jansen C, Marinov GK, Ernst J, Kellis M, et al. Integrating and
1131 mining the chromatin landscape of cell-type specificity using self-organizing maps. Genome
1132 Res. Cold Spring Harbor Lab; 2013;23:2136–2148.

- 1133 30. Hoffman MM, Ernst J, Wilder SP, Kundaje A, Harris RS, Libbrecht M, et al. Integrative
1134 annotation of chromatin elements from ENCODE data. *Nucleic Acids Res. Oxford University*
1135 *Press*; 2013;41:827–841.
- 1136 31. Heintzman ND, Stuart RK, Hon G, Fu Y, Ching CW, Hawkins RD, et al. Distinct and
1137 predictive chromatin signatures of transcriptional promoters and enhancers in the human
1138 genome. *Nat Genet. Nature Publishing Group*; 2007;39:311–318.
- 1139 32. Arneson A, Ernst J. Systematic discovery of conservation states for single-nucleotide
1140 annotation of the human genome. *Commun Biol. Nature Publishing Group*; 2019;2:1–14.
- 1141 33. Abel HJ, Larson DE, Regier AA, Chiang C, Das I, Kanchi KL, et al. Mapping and
1142 characterization of structural variation in 17,795 human genomes. *Nature. Nature Publishing*
1143 *Group*; 2020;583:83–89.
- 1144 34. Cooper GM, Goode DL, Ng SB, Sidow A, Bamshad MJ, Shendure J, et al. Single-nucleotide
1145 evolutionary constraint scores highlight disease-causing mutations. *Nat Methods. Nature*
1146 *Publishing Group*; 2010;7:250–251.
- 1147 35. Di Iulio J, Bartha I, Wong EH, Yu H-C, Lavrenko V, Yang D, et al. The human noncoding
1148 genome defined by genetic diversity. *Nat Genet. Nature Publishing Group*; 2018;50:333–337.
- 1149 36. Fu Y, Liu Z, Lou S, Bedford J, Mu XJ, Yip KY, et al. FunSeq2: a framework for prioritizing
1150 noncoding regulatory variants in cancer. *Genome Biol. BioMed Central*; 2014;15:1–15.

1151 37. Gulko B, Hubisz MJ, Gronau I, Siepel A. A method for calculating probabilities of fitness
1152 consequences for point mutations across the human genome. Nat Genet. Nature Publishing
1153 Group; 2015;47:276–283.

1154 38. Huang Y-F, Gulko B, Siepel A. Fast, scalable prediction of deleterious noncoding variants
1155 from functional and population genomic data. Nat Genet. Nature Publishing Group;
1156 2017;49:618–624.

1157 39. Ioannidis NM, Davis JR, DeGorter MK, Larson NB, McDonnell SK, French AJ, et al. FIRE:
1158 functional inference of genetic variants that regulate gene expression. Bioinformatics. Oxford
1159 University Press; 2017;33:3895–3901.

1160 40. Ionita-Laza I, McCallum K, Xu B, Buxbaum JD. A spectral approach integrating functional
1161 genomic annotations for coding and noncoding variants. Nat Genet. Nature Publishing Group;
1162 2016;48:214.

1163 41. Pollard KS, Hubisz MJ, Rosenbloom KR, Siepel A. Detection of nonneutral substitution rates
1164 on mammalian phylogenies. Genome Res. Cold Spring Harbor Lab; 2010;20:110–121.

1165 42. Quang D, Chen Y, Xie X. DANN: a deep learning approach for annotating the pathogenicity
1166 of genetic variants. Bioinformatics. Oxford University Press; 2015;31:761–763.

1167 43. Rentzsch P, Witten D, Cooper GM, Shendure J, Kircher M. CADD: predicting the
1168 deleteriousness of variants throughout the human genome. Nucleic Acids Res. Oxford University
1169 Press; 2019;47:D886–D894.

- 1170 44. Rogers MF, Shihab HA, Mort M, Cooper DN, Gaunt TR, Campbell C. FATHMM-XF:
1171 accurate prediction of pathogenic point mutations via extended features. *Bioinformatics*. Oxford
1172 University Press; 2018;34:511–513.
- 1173 45. Siepel A, Bejerano G, Pedersen JS, Hinrichs AS, Hou M, Rosenbloom K, et al.
1174 Evolutionarily conserved elements in vertebrate, insect, worm, and yeast genomes. *Genome Res*.
1175 Cold Spring Harbor Lab; 2005;15:1034–1050.
- 1176 46. Smedley D, Schubach M, Jacobsen JO, Köhler S, Zemojtel T, Spielmann M, et al. A whole-
1177 genome analysis framework for effective identification of pathogenic regulatory variants in
1178 Mendelian disease. *Am J Hum Genet*. Elsevier; 2016;99:595–606.
- 1179 47. Karczewski KJ, Francioli LC, Tiao G, Cummings BB, Alföldi J, Wang Q, et al. The
1180 mutational constraint spectrum quantified from variation in 141,456 humans. *Nature*. Nature
1181 Publishing Group; 2020;581:434–43.
- 1182 48. Francioli LC, Polak PP, Koren A, Menelaou A, Chun S, Renkens I, et al. Genome-wide
1183 patterns and properties of de novo mutations in humans. *Nat Genet*. Nature Publishing Group;
1184 2015;47:822–826.
- 1185 49. Lindblad-Toh K, Garber M, Zuk O, Lin MF, Parker BJ, Washietl S, et al. A high-resolution
1186 map of human evolutionary constraint using 29 mammals. *Nature*. Nature Publishing Group;
1187 2011;478:476–482.
- 1188 50. Welter D, MacArthur J, Morales J, Burdett T, Hall P, Junkins H, et al. The NHGRI GWAS
1189 Catalog, a curated resource of SNP-trait associations. *Nucleic Acids Res*. Oxford University
1190 Press; 2014;42:D1001–D1006.

1191 51. Hindorff LA, Sethupathy P, Junkins HA, Ramos EM, Mehta JP, Collins FS, et al. Potential
1192 etiologic and functional implications of genome-wide association loci for human diseases and
1193 traits. *Proc Natl Acad Sci. National Acad Sciences*; 2009;106:9362–9367.

1194 52. Wang J, Huang D, Zhou Y, Yao H, Liu H, Zhai S, et al. CAUSALdb: a database for
1195 disease/trait causal variants identified using summary statistics of genome-wide association
1196 studies. *Nucleic Acids Res. Oxford University Press*; 2020;48:D807–D816.

1197 53. Chen W, Larrabee BR, Ovsyannikova IG, Kennedy RB, Haralambieva IH, Poland GA, et al.
1198 Fine mapping causal variants with an approximate Bayesian method using marginal test
1199 statistics. *Genetics. Genetics Soc America*; 2015;200:719–736.

1200 54. Benner C, Spencer CC, Havulinna AS, Salomaa V, Ripatti S, Pirinen M. FINEMAP:
1201 efficient variable selection using summary data from genome-wide association studies.
1202 *Bioinformatics. Oxford University Press*; 2016;32:1493–1501.

1203 55. Tate JG, Bamford S, Jubb HC, Sondka Z, Beare DM, Bindal N, et al. COSMIC: the
1204 catalogue of somatic mutations in cancer. *Nucleic Acids Res. Oxford University Press*;
1205 2019;47:D941–7.

1206 56. Schuster-Böckler B, Lehner B. Chromatin organization is a major influence on regional
1207 mutation rates in human cancer cells. *nature. Nature Publishing Group*; 2012;488:504–507.

1208 57. Parker SC, Gartner J, Cardenas-Navia I, Wei X, Abaan HO, Ajay SS, et al. Mutational
1209 signatures of de-differentiation in functional non-coding regions of melanoma genomes. *PLoS*
1210 *Genet. Public Library of Science*; 2012;8:e1002871.

- 1211 58. Amemiya HM, Kundaje A, Boyle AP. The ENCODE blacklist: identification of problematic
1212 regions of the genome. Sci Rep. Nature Publishing Group; 2019;9:1–5.
- 1213 59. Harrow J, Frankish A, Gonzalez JM, Tapanari E, Diekhans M, Kokocinski F, et al.
1214 GENCODE: the reference human genome annotation for The ENCODE Project. Genome Res.
1215 Cold Spring Harbor Lab; 2012;22:1760–74.
- 1216 60. Guelen L, Pagie L, Brasset E, Meuleman W, Faza MB, Talhout W, et al. Domain
1217 organization of human chromosomes revealed by mapping of nuclear lamina interactions.
1218 Nature. Nature Publishing Group; 2008;453:948–951.
- 1219
- 1220
- 1221
- 1222
- 1223
- 1224
- 1225